

POLITECNICO DI TORINO

Master's Degree in Aerospace Engineering



**Politecnico
di Torino**

Master's Degree Thesis

**Modeling and Simulation of a Fuel Cell
Electric Vehicle System: Analysis and
Aging Estimation**

Supervisors

Prof. Paolo MAGGIORE

Prof.ssa Manuela BATTIPEDE

Ing. Andrea ALMONDO

Candidate

Giorgio CHIOFALO

July 2023

Summary

With the rise of fuel cell vehicles to mass production, many technical improvements have been realized to drastically increase the range, efficiency, and sustainability of fuel cell vehicles. However, insights into those valuable state-of-the-art solutions are usually not shared with researchers due to the strict non-disclosure policies of fuel cell vehicle manufacturers. Many studies, therefore, rely on assumptions, best-guess estimates, or insider knowledge.

The goal of this thesis work is to presents a comprehensive study on the development and analysis of a Simulink model for a fuel cell bus powered by hydrogen. The research focuses on two main aspects: firstly, the investigation of the electrical behavior of a battery by analyzing data released by Volkswagen for the ID.3 electric vehicle. This analysis provides valuable insights into the battery's State of Charge (SOC), as well as various electrical parameters such as voltage, current and an estimation of the RC parameters of the battery's equivalent electrical circuit.

In addition to this, the thesis explores the State oh Health (SOH) characteristics of the battery by employing a capacity loss model. The aging study aims to understand the degradation of the high power battery over time due to various operational factors.

In the second part of this work, a detailed Simulink model is presented, incorporating the fuel cell system and the previously analyzed battery and also modeling work on the performance and aging of the fuel cell was carried out. The model enables the estimation of the fuel cell bus's performance, considering the interplay between the fuel cell and the integrated battery system.

Finally, aging estimation for both the battery and the fuel cell is provided based on the specific usage patterns derived from the Simulink model. This estimation contributes to a better understanding of the long-term durability and performance of the integrated fuel cell and battery system.

Overall, this thesis offers valuable insights into the electrical behavior, aging characteristics, and performance estimation of a fuel cell bus system with integrated batteries. The methodology and analysis developed in this study can be applied to various types of vehicles, including aerospace applications. By analyzing different driving cycles, this model provides an estimation of essential operating parameters and predicts the remaining life of the battery and fuel cell.

Acknowledgements

Words cannot express my gratitude to my tutor and the guys at PUNCH Hydrocells for their invaluable patience and feedback.

I am also grateful to my colleagues and friends for their help, nightly feedback sessions and immeasurable moral support.

Finally, I would be remiss if I did not mention my family, particularly my parents. Their trust in me kept my spirit and motivation high during this process. I would also like to thank my sister for all the entertainment and emotional support.

Table of Contents

List of Tables	IX
List of Figures	X
Acronyms	XIII
1 Introduction	1
2 Automotive battery overview	3
2.1 Battery pack, modules and cells	5
2.2 Lithium-ion cell	6
2.3 Future of battery cells	11
2.4 Energy oriented vs Power oriented battery	12
3 Lithium-ion battery modelling	14
3.1 Selection of the model	14
3.1.1 Ideal battery model	15
3.1.2 Simple battery model	15
3.1.3 Modified simple battery model	16
3.1.4 Thevenin battery model	17
3.1.5 Modified Thevenin battery model	17
3.1.6 Impedance battery model	18
3.1.7 Runtime-based battery model	19
3.2 Battery model in Simulink	21
3.2.1 SOC Calculation	22
3.2.2 OCV Calculation	22
3.2.3 Thevenin Model	23
3.3 Parameter estimation	24
3.4 Battery degradation factors	26
3.5 Overview of battery aging models	30
3.5.1 Model-based method	30

3.5.2	Data-driven method	31
3.5.3	Hybrid methods	32
3.6	Battery aging model	32
4	Fuel Cell	39
4.1	Proton-exchange membrane fuel cell (PEMFC)	41
4.2	Characteristics and working principles	42
4.3	FC degradation factors	43
4.3.1	Membrane degradation mechanisms	44
4.3.2	Electrocatalyst and catalyst layer	46
4.3.3	Gas diffusion layer	47
4.3.4	Bipolar plate	47
4.3.5	Sealing gasket	48
4.4	FC aging model	49
5	Bus model in Simulink	51
5.1	Driver block	51
5.2	Vehicle controller model	52
5.3	Vehicle dynamic	52
5.4	DC-link	53
5.5	Battery	53
5.6	Energy manager logic	53
5.7	Fuel cell	53
6	Results	64
6.1	SORT 1	64
6.2	SORT 2	67
6.3	Braunschweig	70
6.4	Aging results	73
7	Conclusions	76
A	Matab Script	78
B	Simulink design optimization toolbox	80
C	Driving cycles	81
C.1	Constant driving - 160kph	81
C.2	WLTP	82
C.3	FTP	84
C.4	Urban	85
C.4.1	Interurban	86

C.4.2 Highway	87
Bibliography	89

List of Tables

2.1	Summary of cell components and operating principles	7
3.1	RC parameters	25
3.2	RC parameter mean value	25
3.3	Overview of lithium-ion battery anode aging mechanisms 3.14 . . .	29
3.4	Optimal values of α and β	34
3.5	Optimal values for Urban cycles	34
3.6	Optimal values for Highway cycles	34
4.1	Degradation coefficients	50
4.2	Weight factors values	50
6.1	FC residual lifetime and average speed	74
6.2	Aging mileage for battery and FC	75
6.3	FC residual lifetime in years	75

List of Figures

2.1	Battery cell production in Europe [1]	4
2.2	Cell, module, pack example. (a) Prismatic; (b) Cylindrical	5
2.3	Components of a lithium-ion cell	8
3.1	Ideal battery model	15
3.2	Simple battery model	16
3.3	Modifies simple battery model	17
3.4	Thevenin battery model	18
3.5	Modified Thevenin battery model	18
3.6	Impedance battery model	20
3.7	Runtime-based battery model	20
3.8	Equivalent circuit model in Simulink	21
3.9	SOC model	22
3.10	Open-circuit voltage	23
3.11	Thevenin model	24
3.12	URBAN cycle voltage comparison	26
3.13	HIGHWAY cycle voltage comparison	26
3.14	Degradation mechanism in Li-ion cells [2]	26
3.16	Aging comparison for different aging parameters	35
3.17	Aging comparison for Urban Cycle and different aging parameters	36
3.15	Complete aging model	37
3.18	Battery aging formula represented in Simulink	38
4.1	Electrochemical power sources by year price comparison	40
4.2	Components of Fuel Cell	42
5.1	Complete bus model	54
5.2	Driver	55
5.3	PID model	56
5.4	Vehicle controller	57
5.5	Vehicle dynamic model	58

5.6	Longitudinal vehicle dynamics	59
5.7	DC-link model	60
5.8	Battery model	61
5.9	Energy manager logic model	62
5.10	FC logic	62
5.11	Fuel Cell model	63
6.1	Speed requested vs Vehicle speed - SORT 1	65
6.2	Power balance - SORT 1 (sign convention: +discharge -charge) . . .	66
6.3	Battery parameters - SORT 1 (sign convention: +discharge -charge)	67
6.4	Speed requested vs Vehicle speed - SORT 2	68
6.5	Power balance - SORT 2 (sign convention: +discharge -charge) . . .	69
6.6	Battery parameters - SORT 2 (sign convention: +discharge -charge)	70
6.7	Speed requested vs Vehicle speed - BRAUNSCHWEIG	71
6.8	Battery parameters - BRAUNSCHWEIG (sign convention: +dis- charge -charge)	72
6.9	Power balance - BRAUNSCHWEIG (sign convention: +discharge -charge)	73
6.10	Aging for three different driving cycles Sort 1, Sort 2 ,Braunschweig	74
C.1	Speed profile - Constant driving 160 kph	82
C.2	Speed profile - WLTP	84
C.3	Speed profile - FTP	85
C.4	Speed profile - Urban	86
C.5	Speed profile - Interurban	87
C.6	Speed profile - Highway	88

Acronyms

BMS

Battery Management system

SOC

State of Charge

SOH

State of Health

BEV

Battery electric vehicle

EV

Electric Vehicle

HEV

Hybrid Electric Vehicle

FCEV

Fuel Cell Electric Vehicle

LIB

Lithium-ion Battery

RC

Resistor-Capacitor

DOD

Depth of Discharge

C-rate

Charge or Discharge current divided by nominal capacity

SEI

Solid electrolyte interface

Ea

Activation energy

EOL

End of Life

VW

Volkswagen

WLTP

Worldwide Harmonised Light Vehicles Test Procedure

FTP

Federal test procedure

EPA

Environmental Protection Agency

PEMFC

Proton Exchange Membrane Fuel Cells

ECM

Equivalent circuit model

RUL

Remaining useful life

Chapter 1

Introduction

In recent years, the urgency to address climate change and transition towards sustainable energy sources has reached unprecedented levels. The combustion of fossil fuels for power generation and transportation has contributed significantly to greenhouse gas emissions, exacerbating the environmental challenges we face today. To combat these issues, the development of efficient green energy storage systems has become paramount. Batteries and fuel cells, with their potential to revolutionize power generation and consumption, offer promising solutions to meet the growing energy demands while reducing our carbon footprint.

This thesis focuses on the development of an electric model for a battery and its association with a fuel cell and finally aims to analyze its utilization in practical applications and predict its lifespan. Through battery and fuel cell modelling, this study seeks to exploit the complementary advantages of both technologies.

The transportation sector accounts for a significant portion of global greenhouse gas emissions, prompting the need for greener alternatives. Fuel cells, which utilize hydrogen and oxygen to produce electricity with water vapor as the only byproduct, offer a clean and efficient solution for automotive applications.

The focus of this thesis is to evaluate the performance required for a hybrid FC powertrain with particular focus on its main energy sources, the battery and the FC. Another key aspect of the analysis was the evaluation of the expected life of these components in real life.

The document is organized in the following way:

- Overview of batteries, operating principles and future technologies;
- Battery modelling and aging;

- Overview of fuel cells, operation and aging;
- Bus model (FC + Battery);
- Results and conclusions.

Chapter 2

Automotive battery overview

The shift from traditional combustion engines to electric vehicles and fuel cell vehicles presents a solution to certain issues while also introducing new challenges.

The primary driving factor behind this transition is associated with atmospheric pollution. Emissions from exhaust fumes contain numerous harmful substances such as particulate matter, volatile organic compounds, nitrogen oxides, carbon monoxide, sulfur dioxide, and greenhouse gases. These pollutants not only contribute to various health problems like respiratory infections, heart disease, and lung cancer but also exacerbate global warming and climate change phenomena. To address these concerns, international agreements such as the Kyoto Protocol, Doha Amendment, and Paris Agreement have set common goals, leading to the introduction of Euro standards that aim to regulate vehicle emissions. These standards have progressively become more stringent over time, compelling automakers to find innovative solutions to meet the requirements.

Looking ahead, another significant challenge emerges in the form of population growth. According to United Nations statistics, the world's population is projected to reach 10 billion people within the next 30 years and potentially 12.3 billion people by the end of the century. This demographic trend raises uncertainties and necessitates appropriate management. Population growth not only amplifies the environmental impact of human activities globally, as indicated by the Global Footprint Network [3], but also demands the exploration of more efficient means of transportation for people and goods.

Fuel cell and electric vehicles offer a partial solution to these problems. While

Automotive battery overview

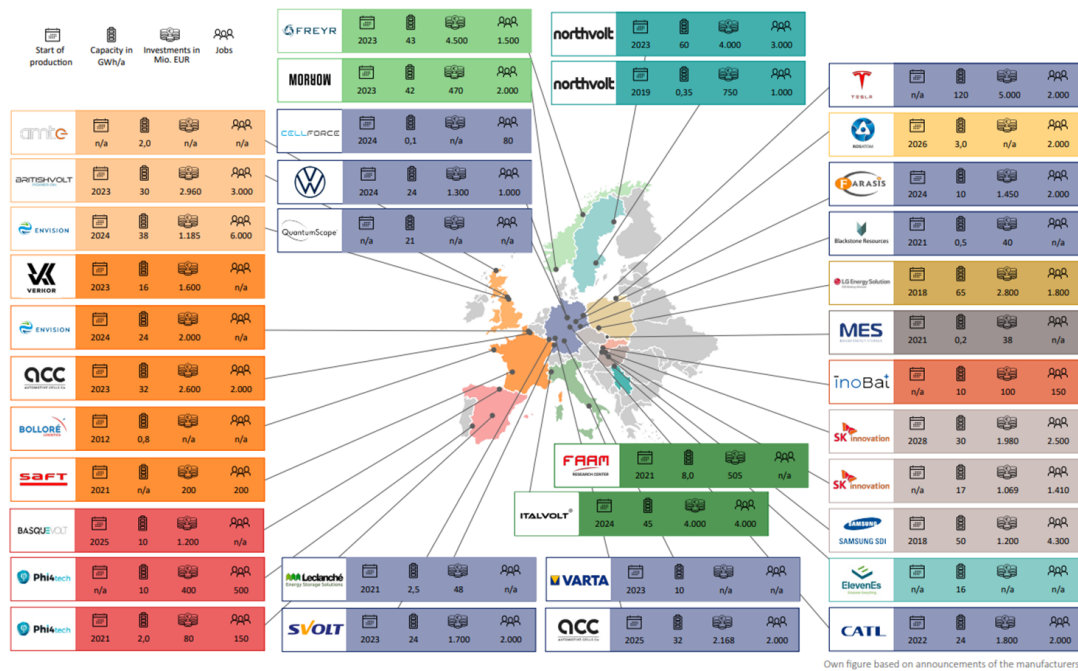


Figure 2.1: Battery cell production in Europe [1]

their production poses ecological challenges, their usage eliminates the issue of air pollution and can contribute to a transportation revolution.

The gradual phasing out of fossil fuels is counterbalanced by the adoption of alternative energy storages, such as lithium-ion batteries. The main features of these batteries are: high energy density, lightweight nature, long lifespan, and low production costs, compared to lead acid battery, making them a common component in most electric vehicles.

This trend can be justified by the large investments in cell production worldwide. 2.1 gives an overview of the plants already in operation and the opening of new ones in the European landscape.

To ensure their optimal utilization, a battery management system (BMS), is responsible for overseeing battery operations. To achieve this, the BMS must estimate two fundamental parameters: the state of charge (SOC) and the state of health (SOH) of the battery. While accurately predicting these quantities in real-time driving scenarios is challenging, doing so enhances vehicle performance and extends the driving range. Consequently, SOC and SOH estimation has gained substantial industrial importance and has become a prominent research area in the

past decade.

2.1 Battery pack, modules and cells

The battery cell serves as the fundamental building block of a battery pack, generating an electric potential dependent on the electrode chemistry and operating conditions, such as temperature and state of charge.

Within a cell, electric charge can be stored and discharged to an external circuit. The nominal charge capacity indicates the maximum amount of charge a cell can hold.

Electrochemical energy is stored in the cell and converted into electrical energy when connected to a load. Ongoing research focuses on improving specific energy and energy density to achieve lighter and smaller batteries. Specific energy refers to the maximum amount of energy stored per unit weight, while energy density represents the energy stored per unit volume.

Batteries can be connected in series or parallel configurations to achieve higher voltage or higher capacity, respectively. Multiple cells combined form a battery module.

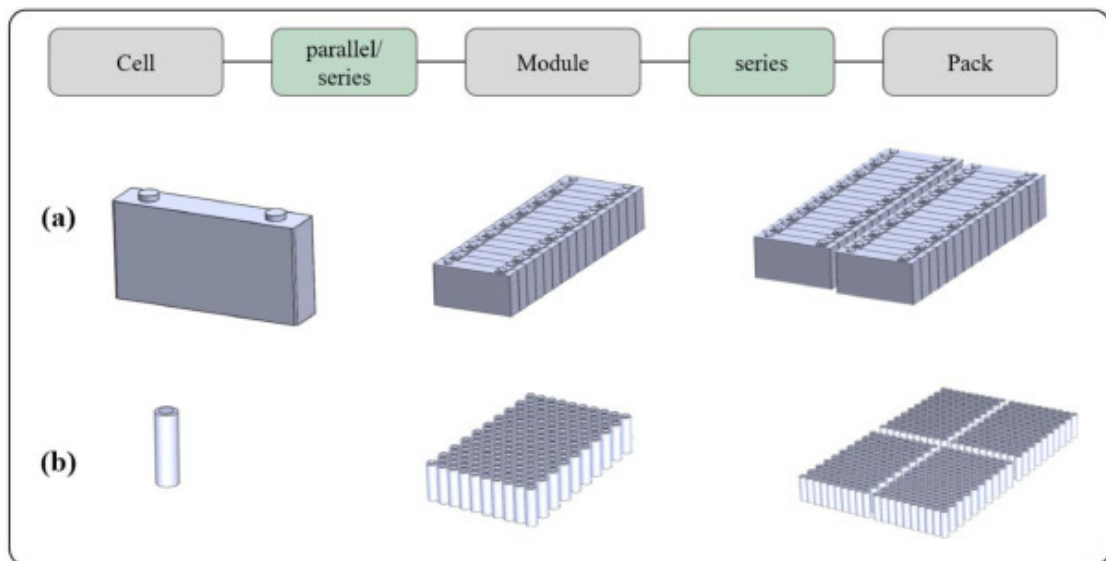


Figure 2.2: Cell, module, pack example. (a) Prismatic; (b) Cylindrical

Battery cells can be interconnected to form additional modules, creating a battery pack 2.2. Different shapes of battery cells exist, including cylindrical, prismatic, and pouch. In cylindrical and prismatic cells, elongated foils of positive

and negative electrodes are separated by a separator and wound around a mandrel. Pouch cells, on the other hand, feature a stacked structure where positive and negative electrodes alternate with separators between each layer. Prismatic and pouch cells are advantageous for space utilization, while the spacing between cylindrical cells aids in thermal management.

2.2 Lithium-ion cell

In recent decades, lithium-ion batteries have revolutionized the battery industry, emerging as a primary source of energy storage for various applications, including portable electronics, electric vehicles, and grid energy storage. Their unique characteristics and performance have propelled them to the forefront of battery technology, making them a crucial area of research and development. The aim of this thesis is to explore the functioning and characteristics of lithium-ion cells, providing a comprehensive overview of their working principles, construction, and key features.

A cell comprises several components, including a positive electrode, a negative electrode, corresponding current collectors, an electrolyte, and a separator. The positive and negative current collectors serve as connection points with the external circuit. Charging and discharging processes rely on redox reactions. The negative electrode acts as the region where charge accumulates within the cell. During discharging, electrons are released through an oxidation reaction, flowing towards the external circuit. Hence, the negative electrode is also known as the anode. Electrons reach the positive electrode (cathode), where a reduction reaction occurs. During charging, electrons are driven from the positive electrode to the negative electrode, now referred to as the anode and cathode, respectively. The electrolyte plays a crucial role in facilitating the transfer of ions between the two electrodes, while the separator acts as both an electrical insulator, preventing short circuits, and a good conductor for ions. This can be observed in 2.3.

The cathode primarily consists of lithium-based compounds such as lithium cobalt oxide (LiCoO_2) or lithium iron phosphate (LiFePO_4), while the anode comprises a carbon-based material, typically graphite. Facilitating the movement of lithium ions, the electrolyte usually constitutes a lithium salt dissolved in an organic solvent.

Charging involves extracting lithium ions from the cathode, moving them through the electrolyte, and intercalating them into the anode material (commonly graphite), thereby storing energy in the anode. Conversely, during discharging, lithium ions are released from the anode, migrating back to the cathode, and delivering electrical energy to an external circuit.

Table 2.1: Summary of cell components and operating principles

Battery components	Typical composition	Function
Cathode	Lithium, Nickel, Cobalt, Manganese, Aluminum, Iron, and Phosphate	Contributing Li-ions through the channel of electrolyte and electrons to be stored at anode side
Anode	Graphite, Silicon (Si)	Keeping Li-ions stored when battery is charged and releasing Li-ions and electrons back to cathode when discharged
Separator	Polyethylene (PE)	Keeping cathode and anode materials separated while allowing Li-ions capable of travelling between them
Current collector (Cathode)	Aluminum (Al)	Collecting electrons generated from the electrochemical reaction at the cathode side while preventing it from being oxidized by cathode materials
Current collector (Anode)	Copper (Cu)	Collecting electrons generated from the reaction at the anode side while preventing it from being oxidized by anode materials
Electrolyte	Solvents (EC, DMC, DEC, EMC, PC, and etc.); Salts (LiPF ₆ , LiClO ₄ , LiBF ₄ , and etc.)	Providing Li-ions with a good conductivity while maintaining a good thermal stability and a wide operable voltage window

PARTS OF A LITHIUM-ION BATTERY

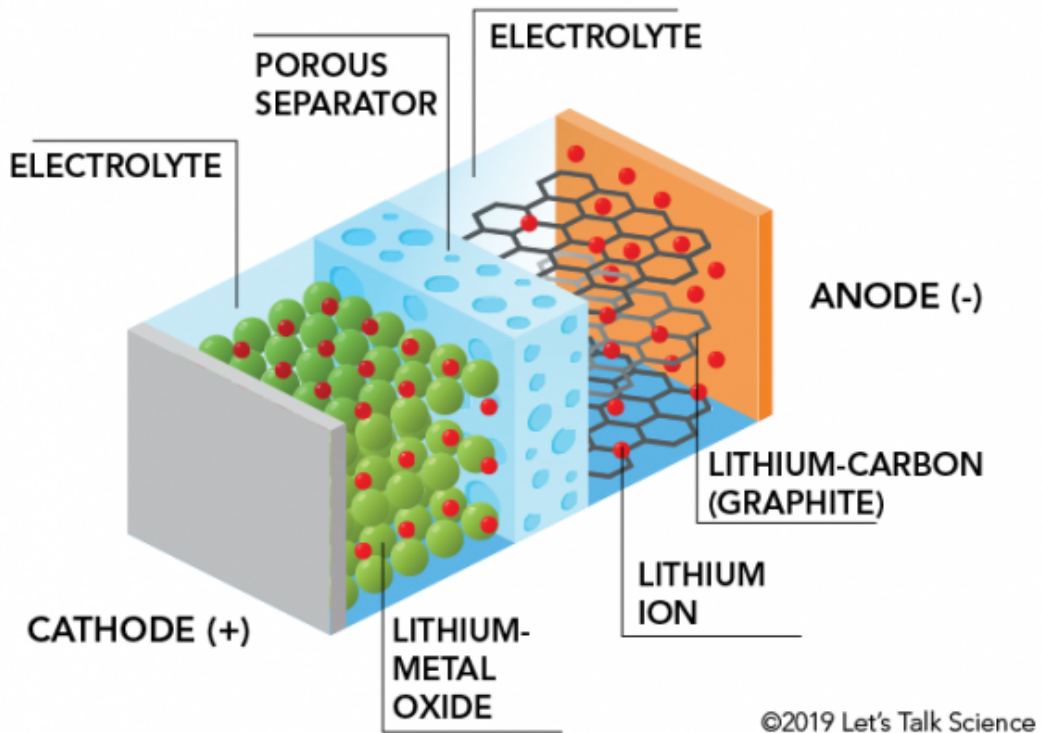


Figure 2.3: Components of a lithium-ion cell

Electrochemical reactions occur at the electrodes during the charging and discharging processes of a lithium-ion cell. At the cathode, lithium ions undergo oxidation, while transition metal ions (e.g., Co_3^+ in LiCoO_2) experience reduction, resulting in the release of electrons. This establishes a potential difference, facilitating the flow of electrons through an external circuit and generating electrical energy. At the anode, lithium ions undergo reduction, leading to the intercalation and storage of lithium ions within the anode material. The reversible electrochemical reactions of lithium-ion cells enable their repeated charging and discharging cycles. An overview of the various components of a cell and how they function is shown in 2.1.

Li-ion cells have several remarkable characteristics contributing to their widespread

adoption. A key feature is their high energy density, which denotes the amount of energy stored per unit mass or volume. Compared to other conventional rechargeable battery technologies, Li-ion cells offer superior energy density. This makes them highly desirable for applications where lightweight and compact energy sources are crucial.

Another advantageous attribute of Li-ion cells is their long cycle life, meaning they can endure numerous charge and discharge cycles before experiencing significant capacity degradation. This longevity is attributed to the reversible nature of the electrochemical reactions at the electrodes and the use of stable electrode materials.

Li-ion cells also exhibit a low self-discharge rate, meaning they retain a substantial portion of their stored energy even when not in use over extended periods. Consequently, they are well-suited for applications requiring long shelf life.

The cathode material typically identifies a Li-ion battery cell. While the anode material is traditionally based on carbon (such as graphite or coke), emerging materials like lithium metal alloys, metal-based alloys, C composites, and lithium titanium oxide are gaining prominence. In commercial batteries, there are four primary cathode materials used:

- LiCoO_2 (LCO - Lithium Cobalt Oxide)
- LiNiO_2 (LNO - Lithium Nickel Oxide)
- LiMn_2O_4 (LMO - Lithium Manganese Oxide)
- LiFePO_4 (LFP - Lithium Iron Phosphate)

LCO was the initial material used and has a high capacity, making it common in consumer batteries. However, its use of expensive cobalt as a cathode material poses a cost concern. LCO has a layered crystal structure.

LNO offers the best capacity and power, but its unstable layered crystalline structure results in reduced lifetime and low thermal stability.

In contrast, manganese oxide (LMO) is known for its stability due to a different crystal structure called spinel, which is more stable and has minimal excess lithium ions in the fully charged state. This minimizes the deposition of undesirable lithium metal on the negative electrode during overcharge. Additionally, the threshold for thermal decomposition of the charged material is higher compared to the previous materials. However, LMO dissolves in the electrolyte at temperatures above ambient. This issue can be mitigated by adding foreign ions and an oxide coating.

For automotive batteries, a combination of the first three materials is used, resulting in the following compositions:

- $\text{LiNi}_{0.85}\text{Co}_{0.1}\text{Al}_{0.05}\text{O}_2$ or NCA (Lithium nickel cobalt aluminium oxides)

- $\text{LiNi}_x\text{Co}_y\text{Mn}_z\text{O}_2$ or NMC (Lithium nickel manganese cobalt oxides)

NCA exhibits favorable power and capacity characteristics similar to LiNiO_2 but at a lower cost than LiCoO_2 . The addition of Aluminum prevents a phase change in the crystalline structure, which depends on the Li-concentration, and minimizes volume changes. However, NCA cathodes have safety concerns and high costs. They are the most thermally unstable among automotive Li-ion chemistries, degrading at high charge levels and low charge levels due to a change in crystal shape. To address safety and lifespan concerns, engineering measures such as separators, cooling systems, and control mechanisms to prevent over-discharge and overcharge have been implemented.

To overcome the safety and cost concerns associated with NCA, NMC batteries have been developed. Various compositions are possible, combining the capacity of LiCoO_2 , the safety of LiMnO_2 , and the capacity and power of LiNiO_2 . The most popular composition is the 1-1-1 ratio or $\text{LiNi}_{1/3}\text{Co}_{1/3}\text{Mn}_{1/3}\text{O}_2$. Nickel also stabilizes the crystal structure in the discharged state, improving the cycle life. While this chemistry helps reduce costs and is believed to be safer, challenges remain in terms of cycle life at high charging, safety, and cost.

Some companies advocate for the use of LiMn_2O_4 in combination with a different anode material called lithium titanate oxide (LMO + LTO) instead of the usual graphite anodes. This combination offers the advantage of lithium titanate oxide not reacting adversely with commonly used electrolytes in Li-ion cells, eliminating the need for a passivation layer. The resulting batteries become more stable, charge quickly even at low temperatures, have a long lifespan, and a wider range of their capacity can be utilized (0-100% charge). However, lithium titanate batteries contain less energy as they operate nominally at approximately 2.5 V, which is lower than the around 3.6 V for the previously mentioned chemistries. This may require automakers to use more cells of this type, potentially increasing the cost compared to NMC batteries. This technology is suitable for applications that require ultra-long life, low energy but high power, such as hybrid electric vehicles (HEVs) or fuel cell vehicles (FCVs).

Lithiated iron phosphate (LFP) is the newest cathode material among the four mentioned, utilizing cheaper materials compared to the previous cathodes. It belongs to the polyanions and has an olivine crystal structure. LFP has a lower electrochemical potential compared to NCA and NCM, making it less likely to oxidize the electrolyte solvent and thus more stable, especially at high temperatures. Its nominal potential is approximately 3.2 V. Advancements have addressed the initially poor electron conductivity by coating the particles with carbon to facilitate electron movement and doping the material to modify its electronic structure. LFP cathodes are inherently safer and more resistant to overcharging compared to

previous materials due to their highest thermal decomposition temperature and lowest energy release. However, LFP batteries may exhibit weaker performance in cold weather and could pose challenges for electronic monitoring due to their almost flat potential curve as the state of charge changes. The flat curve results from a phase change occurring in the material during discharge or charge, which keeps the potential nearly constant. Additionally, LFP batteries have a lower volumetric energy density compared to NMC materials, which can be a drawback for their use in electric vehicles (EVs) [4].

2.3 Future of battery cells

In this paragraph, we will explore the future technologies of batteries for electric vehicles (EVs). As the demand for EVs continues to rise, advancements in battery technology are crucial for enhancing their performance, range, and overall sustainability. Researchers and engineers are tirelessly working to develop innovative solutions that can revolutionize the EV industry. This section will investigate into some of the promising technologies on the horizon, discussing their potential to overcome current limitations and shape the future of electric mobility.

The future of Li-ion battery technology is based on three specific technological advancements. Improvements in battery technology can be achieved in a huge range of different ways and focus on several different components to deliver certain performance characteristics of the battery. While there are various paths that battery technology evolution could take, S&P Global [5] has defined three new alternatives to lithium-ion batteries:

- Current commercial LIB: Most favorable technologies for today's EV and stationary energy storage applications.
 - Cathode material: NMC 532, NMC 622, NCA, or LFP;
 - Anode material: artificial graphite or natural graphite;
 - Electrolyte: carbonate-based liquid organic solvents;
 - Current collector: Cu and Al foils.

- Advanced LIB: Most likely to be adopted on light vehicle EVs that require longer ranges and fast charging:
 - Cathode material: NMC 811 or NCA 90;
 - Anode material: natural/artificial graphite with SiOx or pure Si;
 - Electrolyte: carbonate-based liquid organic solvents;

- Separator: Polymer thin films;
- Current collector: Cu and Al foils.
- Solid-state: Key technology to eliminate battery fire concerns and deliver moderate performance improvements:
 - Cathode material: NMC 811, NCA 90, LNMO (high-voltage);
 - Anode material: graphite with large amount of pure Si or Li-metal;
 - Electrolyte: ceramic, polymer or sulphur-based solid electrolyte;
 - Separator: as part of solid-state electrolyte;
 - Current collector: Cu and Al foils.
- Lithium Sulphur/Air: Revolutionary technologies that diverge from all previous chemistry systems:
 - Cathode material: Li-metal;
 - Anode material: Sulphur or Oxygen/Air;
 - Electrolyte: solid-state;
 - Separator: as part of solid-state electrolyte;
 - Current collector: Porous carbonaceous material, noble metal catalysts, and Cu foil.

2.4 Energy oriented vs Power oriented battery

In the field of energy storage, batteries play a pivotal role in providing portable power for various applications. As technology continues to advance, battery systems have evolved to cater to different needs and requirements. Two prominent categories of batteries are energy-oriented and power-oriented batteries. While both serve the purpose of energy storage, they differ significantly in their design, characteristics, and performance parameters. This section aims to elucidate the disparities between energy-oriented and power-oriented batteries, shedding light on their distinct features and applications.

Energy-oriented batteries, as the name suggests, are primarily designed to store and deliver a high amount of energy over an extended period. These batteries prioritize energy density, which refers to the amount of energy that can be stored per unit volume or weight. Energy-oriented batteries typically have higher energy densities compared to power-oriented batteries, enabling them to store a larger amount of energy.

These batteries are characterized by their slow discharge rates and relatively low power output. Due to their emphasis on energy storage, energy-oriented batteries can deliver a sustained power supply over a prolonged duration. They are commonly used in applications where long-lasting power is required, such as electric vehicles for extended-range driving, renewable energy storage systems, and grid-level energy storage.

In contrast to energy-oriented batteries, power-oriented batteries are designed to deliver a high amount of power in a short duration. These batteries prioritize power density, which refers to the rate at which energy can be delivered from the battery. Power-oriented batteries exhibit higher power densities compared to energy-oriented batteries, allowing them to provide a quick burst of power when needed.

Power-oriented batteries are characterized by their high discharge rates and the ability to deliver a substantial amount of power instantaneously. They find applications in scenarios where high-power demands are prevalent, such as electric vehicles for acceleration and heavy machinery. Additionally, power-oriented batteries are often utilized in applications that require rapid charging and discharging, such as portable electronics and energy storage systems for peak shaving.

In summary, energy-oriented and power-oriented batteries serve distinct purposes in the realm of energy storage. Energy-oriented batteries prioritize energy density, offering extended energy storage and slow discharge rates. They find applications in scenarios that require sustained power supply over a longer duration. On the other hand, power-oriented batteries prioritize power density, delivering high power outputs and rapid charging capabilities. They are suitable for applications that demand quick bursts of power and fast charging/discharging cycles. Understanding the differences between these battery types is crucial for selecting the most appropriate energy storage solution based on specific requirements and performance expectations. State-of-the-art NMC (nickel-manganese-cobalt) batteries are used for energy-oriented batteries. For power-oriented batteries, more LTO (lithium titanate oxide) solutions are used for high performance but high cost. Chemicals such as NMC or LFP can be used to reduce costs.

Chapter 3

Lithium-ion battery modelling

To ensure the safe and reliable operation of the entire battery energy storage system, a battery management system (BMS) is necessary to estimate and predict the state of charge (SOC) and state of health (SOH) of the lithium-ion battery. In order to accurately estimate the state of the lithium-ion battery, it is crucial to establish a precise battery model.

Currently, there are three widely used models for lithium-ion batteries: the electrochemical model, the equivalent circuit model, and the neural network model [6]. The equivalent circuit model replicates the nonlinear operating characteristics of lithium-ion batteries using circuit elements that have adjustable parameters such as resistance, capacitance, and voltage source. This model is extensively employed. To create an accurate equivalent circuit model for the battery, it is necessary to precisely determine the parameter values for the circuit components. Typically, different SOC values correspond to different sets of model parameters.

3.1 Selection of the model

Battery modeling involves three categories of modeling: electrochemical modeling, electrical circuit modeling and neural network model. The electrochemical model of a battery is structurally based on the internal electrochemical actions and reactions of a cell. It is not derived from an electrical network. While this model is accurate, it is complex and requires a precise understanding of the electrochemical processes within the cell. It is not suitable for power and dynamic systems studies. On the other hand, electrical circuit modeling is another useful model that has been presented by many researchers. In electrical circuit modeling, the electrical characteristics of the battery are considered, and passive linear elements are used.

Such models are easy to comprehend. For instance, the battery capacity can be modeled by a capacitor. Since the voltage and internal resistance of a battery depend on temperature and state of charge, the open circuit voltage of a battery, represented by a controlled DC voltage source, changes with the state of charge and temperature. Moreover, the internal resistance is modeled by a variable resistance. The value of the internal resistance is also influenced by the state of charge and temperature. The neural network model will not be seen in detail.

In this paragraph, the electrical circuit models are categorized into four overall models. These models include simple models, Thevenin-based models, impedance-based models and runtime-based models. The specifications and applications of each model are considered and discussed. Finally, the advantages and disadvantages of each model are presented below.

3.1.1 Ideal battery model

The simplest model of an ideal battery neglects internal parameters and is represented by only an ideal voltage source. This model, shown in 3.1, is mainly suitable for simulations where the energy released from the battery is assumed to be infinite. The state of charge and internal parameters of the battery are not taken into consideration in this model [6].



Figure 3.1: Ideal battery model

3.1.2 Simple battery model

A simplified battery model, as shown in 3.2, consists of a series of internal resistances connected to an ideal voltage source. The state of charge (SOC) is not considered

in this model. In the figure, V_0 represents the ideal open-circuit voltage, V_t is the terminal voltage of the battery, and R_{int} is the internal series resistance. In this simple battery model, the terminal voltage V_t can be determined through an open circuit voltage measurement test. The internal resistance R_{int} is assumed to be constant, but it changes when a load is connected to the battery. Therefore, this model is only suitable for circuit simulations where the energy released from the battery is assumed to be infinite, and the state of charge is not important. For instance, this model is not suitable for applications such as electric trains or vehicles. However, it can be used in conjunction with ultra-capacitors or fuel cells as hybrid energy storage. Additionally, this model is applied as an input source connected to inverter power electronic devices [6].

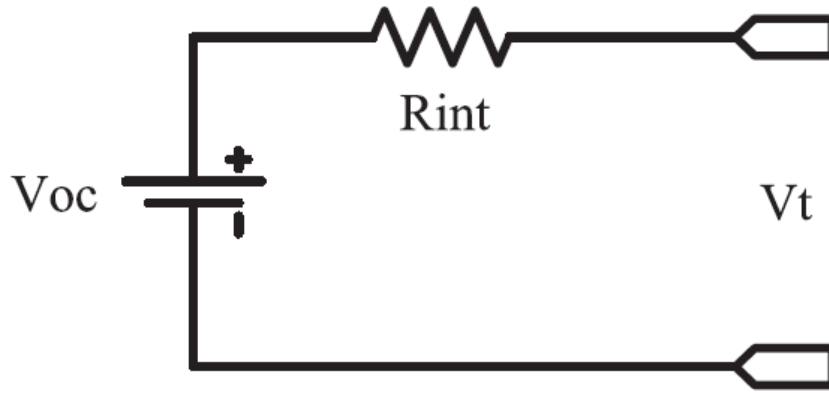


Figure 3.2: Simple battery model

3.1.3 Modified simple battery model

In this model, illustrated in 3.3, the battery is utilized as a voltage source connected to a series resistance. The voltage and internal resistance are both dependent on the state of charge (SOC). The terminal voltage can be defined as follows:

$$V_t = V_{oc}(SOC) - IR_{int}(SOC) \quad (3.1)$$

where $V_{oc} = f(SOC)$ is in the open circuit voltage of the battery and $R_{int} = f(SOC)$ is the internal resistances of discharges and charge cycles, where:

$$V_{oc} = V_0 - A \cdot D \quad (3.2)$$

$$R_{int} = R_0 - B \cdot D \quad (3.3)$$

where V_0 is open circuit voltage (battery is in full charge), D is the state of discharge, R_0 is the internal resistance (battery is in full charge), and A , B are

constants determined through experiments. It is important to note that this model does not consider the transient condition. This model is commonly used in single-phase inverter systems to convert a DC voltage into an alternative voltage to meet the power requirements of an AC load, such as an induction motor [6].

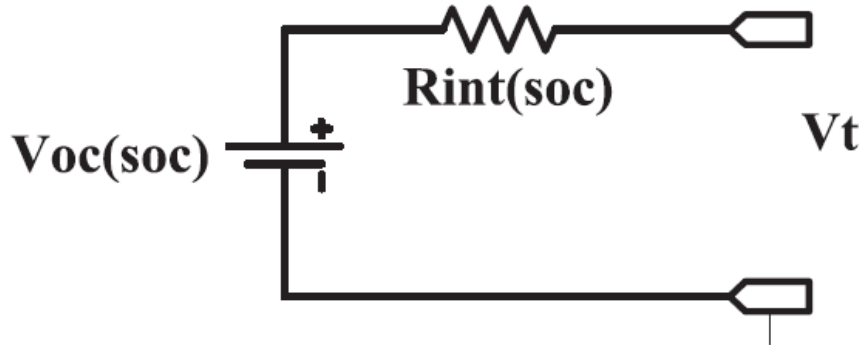


Figure 3.3: Modifies simple battery model

3.1.4 Thevenin battery model

The transient behavior of the battery has not been investigated in the previous models. The Thevenin battery model consists of an ideal voltage source (V_0), an internal resistance (R_{int}), an overvoltage resistance (R_1), and a capacitor (C_1). The configuration of this model is shown in 3.4. C_1 acts as a temporary energy storage device in an RC circuit, and R_1 represents the resistance associated with the contact resistance of the plate. However, a major limitation of the Thevenin battery model is that all parameter values are assumed to be constant, whereas in reality, these parameter values are related to the state of charge (SOC), storage capacity of the battery, discharge rate, temperature and some other characteristics of discharge. The application of this model is in hybrid power train modeling where the battery is combined with fuel cell/ultra capacitor energy storages [6].

3.1.5 Modified Thevenin battery model

This model incorporates the transient behavior of a battery, which consists of an RC parallel network. In this network, R_1 represents the overvoltage resistance, and C_1 represents the double-layer capacitance. Additionally, there is an ohmic resistance, R_{int} , that accounts for the instantaneous voltage drop, as depicted in 3.5. It's important to note that this model cannot predict the battery runtime, nor can it model the DC response of the battery cell.

The open-circuit voltage, V_{oc} , is related to the state of charge (SOC) [6].

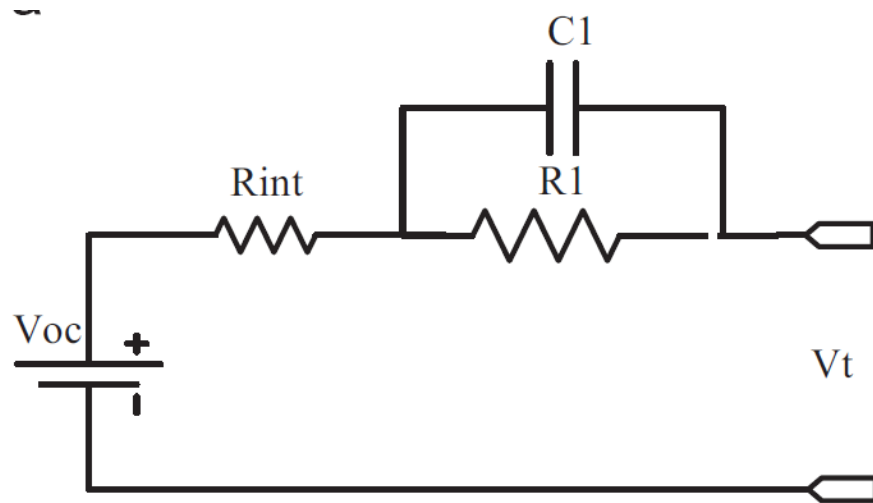


Figure 3.4: Thevenin battery model

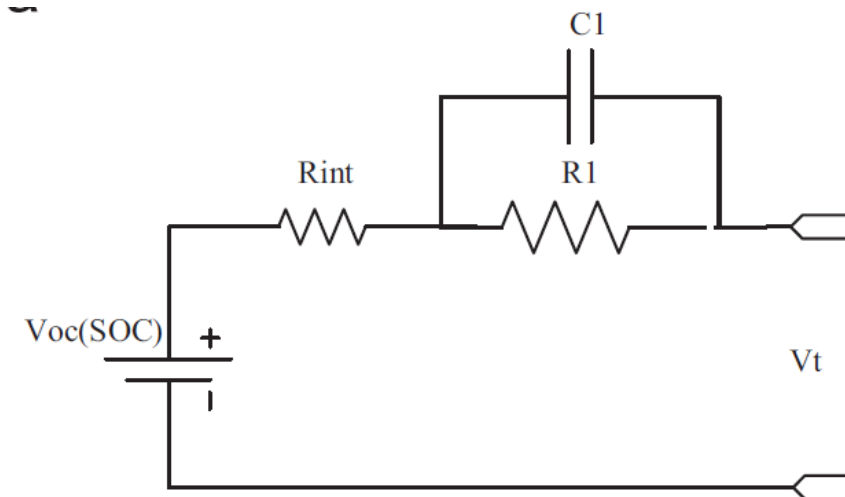


Figure 3.5: Modified Thevenin battery model

3.1.6 Impedance battery model

The impedance-based model, illustrated in 3.6, is an electrical model that utilizes electrochemical impedance spectroscopy (EIS) measurements to capture the AC response of a cell at specific frequency ranges. The impedance elements in this model are determined through EIS measurements, which are represented on a Nyquist diagram. The Nyquist diagram consists of a real axis representing cell resistance and an imaginary axis representing cell reactance. Each point on this

diagram represents the impedance response at a specific frequency.

To achieve the impedance response, a small-amplitude sinusoidal current or voltage signal is applied to the system, and the response is analyzed at different frequencies. This method is employed to keep the system in the linear region, ensuring a sinusoidal response with varying amplitudes and phase angles. The internal impedance of the battery, which is influenced by electrochemical processes, is modeled using the Randle circuit depicted in 3.6.

In this model, R_{int} represents the bulk resistance, describing the electrical conductivity of the electrodes and separator. RSE and CSE represent the resistance and capacitance of the surface film layer on the electrodes, respectively. R_{ct} denotes the charge transfer resistance, which relates to the charge transfer between the electrode and the electrolyte. C_{dl} represents the double-layer capacitance between the electrode and electrolyte, demonstrating the medium-frequency response. ZW represents the Warburg impedance, which reflects the diffusion of lithium ions between the electrolyte and active material in lithium-ion batteries, particularly at low frequencies.

To enhance the accuracy of the model, an RC pair is included, which can be replaced with a resistance when high accuracy is not essential. Additionally, in some cases, an inductance is incorporated in series with the bulk resistance to explain the positive reactance response at high frequencies. However, the positive reactance response can often be neglected. This model finds application in modeling and simulating traction electric/hybrid vehicles [6].

3.1.7 Runtime-based battery model

The 3.7 illustrates the runtime-based circuit model, which is the equivalent circuit of a battery cell. This model is designed to simulate the runtime and DC response of the battery under a constant discharge current. It can also be utilized for limited transient responses. The model takes into account the following effects:

- The battery voltage is dependent on the state of charge (SOC). As the battery is discharged, the voltage, V_t , decreases at a varying rate.
- The actual capacity of the battery is influenced by the discharge rate. The conversion of chemical energy into electrical energy diminishes as the discharge rate increases.
- The total charge quantity is affected by the discharge current frequency.

The runtime-based circuit model consists of three separate circuits. The left circuit represents the dependence on the discharge frequency. It includes elements R_0 , C_0 , and V_{c-rate} . R_0 and C_0 are transient elements referred to as charge storage

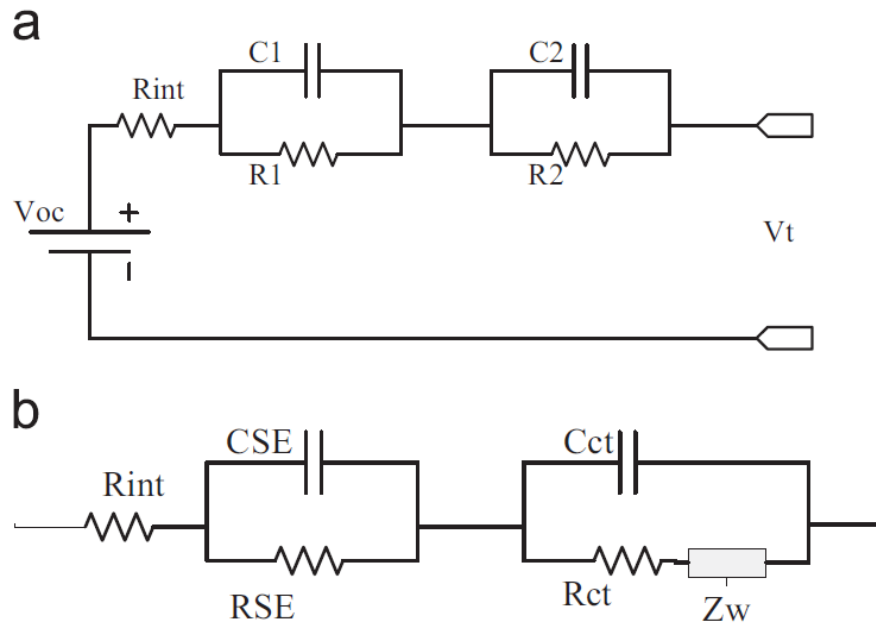


Figure 3.6: Impedance battery model

resistor and charge storage capacitor, respectively. They form a low-pass filter that controls V_{lost} .

The middle circuit represents the dependence on the state of charge and discharge rate. It includes elements V_{lost} , C_{bat} , R_{sdis} , and a current source I_b . V_{lost} accounts for the dependence on the discharge rate and controls the battery charge and the output voltage. Its magnitude is determined using a lookup table. C_{bat} represents the battery capacitor, and R_{sdis} represents the self-discharge resistor.

Finally, the right circuit includes the open circuit voltage (V_{oc}) and the internal resistor of the battery (R_{int}). This model has found application in the modeling of traction electric/hybrid vehicles [6].

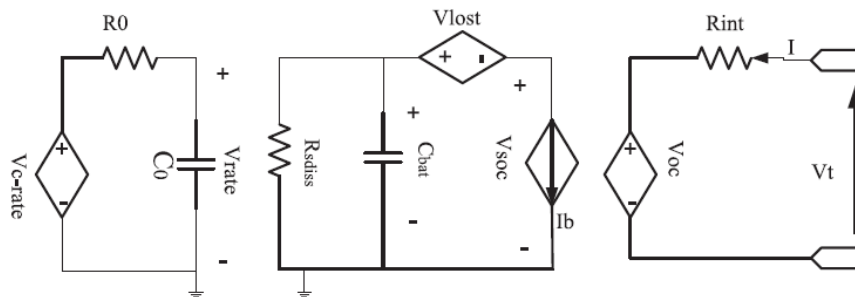


Figure 3.7: Runtime-based battery model

3.2 Battery model in Simulink

Accurate battery information, such as state-of-charge (SOC), current, and voltage, is crucial for circuit designers to effectively manage energy consumption in battery-powered systems. It is also essential to handle batteries properly to prevent overcharging or over-discharging. Therefore, having an accurate battery model is vital during the circuit design process to forecast battery characteristics.

For this thesis, data published by Volkswagen regarding its studies for the ID.3 was used [7]. This dataset includes an 11 Gb teardown in which the characterisation of the battery with the development of its main parameters is presented. Some of the data of this teardown have not been made public, such as the trend of the various parameters under varying temperatures. In fact, the main assumption in the thesis work will be the constant temperature in all driving cycles.

The battery will be approximated with an equivalent electrical circuit such as the modified Thevenin battery model shown in 3.8. This model is an excellent trade-off between accuracy and computational effort.

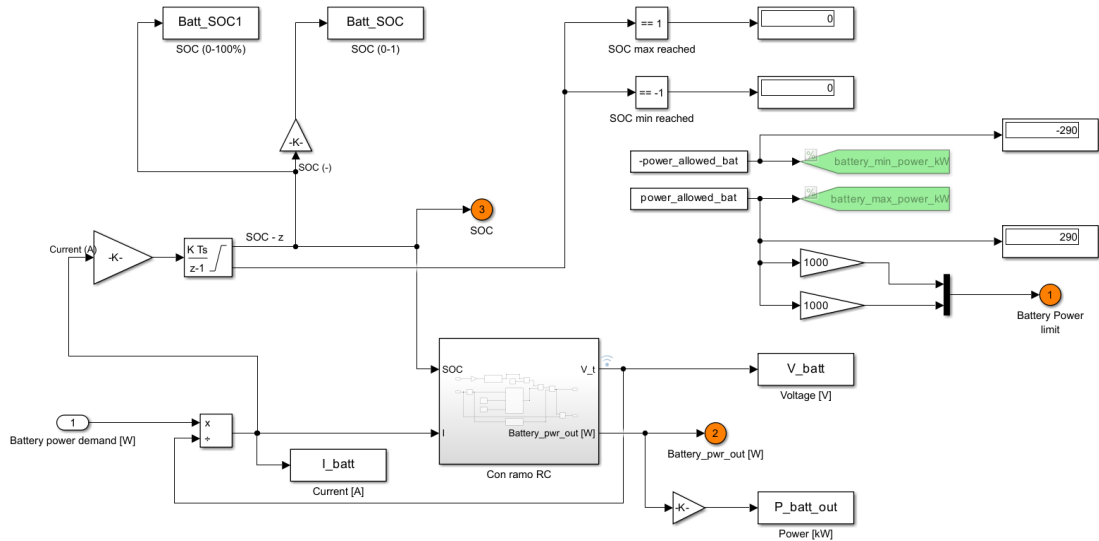


Figure 3.8: Equivalent circuit model in Simulink

The power demanded by the battery is the input signal of the model, which after being divided by the voltage, yielding the current, will be the input of thevenin electrical model seen above. Then the current SOC is calculated at each iteration in the block called "SOC" found in 3.9, which will then be the input for the equivalent

electrical circuit. In the "Thevenin Model" block, the behavior of the battery will be modeled.

3.2.1 SOC Calculation

The model in 3.9 implements an estimator that calculates the state-of-charge (SOC) of a battery by using the Coulomb counting method. There are two inputs in this subsystem, one is initial SOC (SOC_0) and another one is current (I). The output of this subsystem is the real time SOC.

$$SOC(t) = SOC(t - 1) + \int_0^t \frac{I}{C_{batt}} dt \quad (3.4)$$

where I is the battery current, in Ampere [A] , and C_{batt} is the nominal battery capacity, in Ampere-hour [A · hr].

In the full battery model, shown in 3.8, the SOC calculation is done in a Gain block but could be displayed as in 3.9.

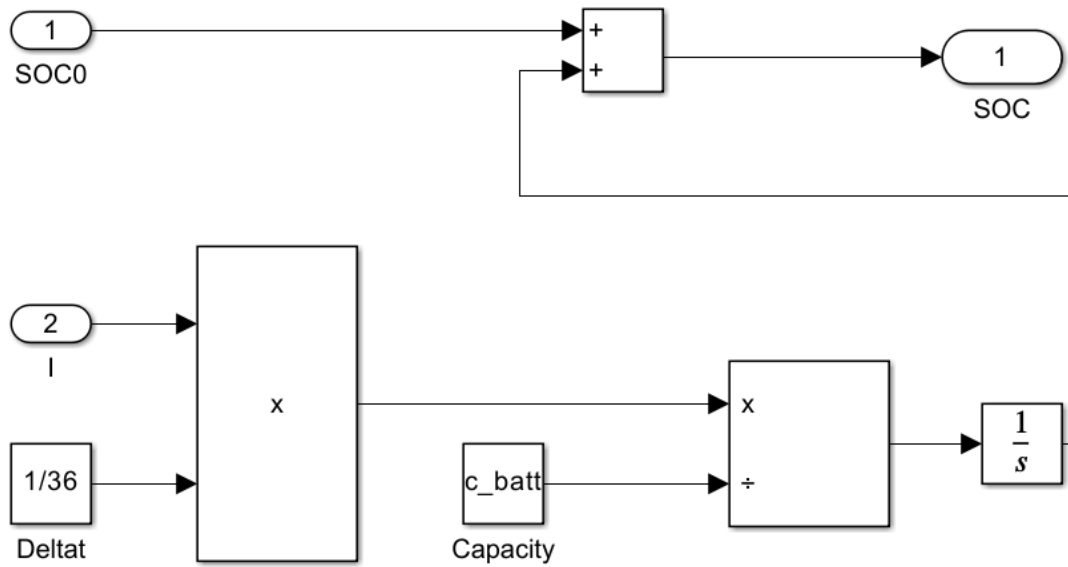


Figure 3.9: SOC model

3.2.2 OCV Calculation

Open circuit voltage is the voltage of battery during equilibrium state. It is one of the important parameter to be realized. OCV is calculated through a look-up table according to the current SOC. The data of the OCV is taken from the VW

ID.3 article [7] and is presented in 3.10, in which in abscissae is the SOC in % and in ordinates the battery pack voltage in V.

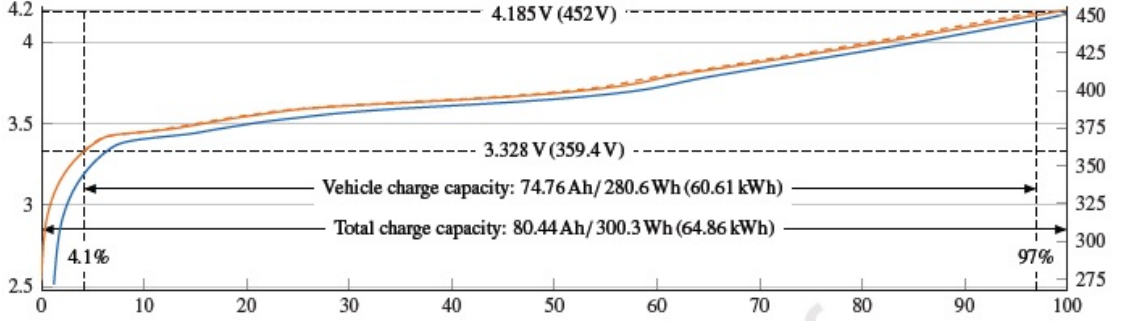


Figure 3.10: Open-circuit voltage

3.2.3 Thevenin Model

In the block of the "Thevenin model", presented in 3.11, the characterization of the electrical parameters of the battery takes place. Parameters R_0 , R_1 , and C_1 , are assumed constant because no temperature dependence is included in the model, and the only dependence on SOC is negligible. Their value was estimated through the use of the "Simulink Design Optimization Toolbox" which will be seen in more detail in the next section.

The voltages of RC parallel networks are corresponding to transient response of battery voltage. By using s-domain, the voltage of RC parallel network can be expressed as below:

$$V_1 = \left(\frac{1}{s}\right) \left[\frac{I}{C} - \frac{V}{RC}\right] \quad (3.5)$$

While V_s , the internal resistance voltage, can simply be written as:

$$V_s = I \cdot R_0 \quad (3.6)$$

which is finally aimed at finding the voltage at the ends of the battery V_t , with reference to 3.5, as:

$$V_t = OCV - V_1 - V_s \quad (3.7)$$

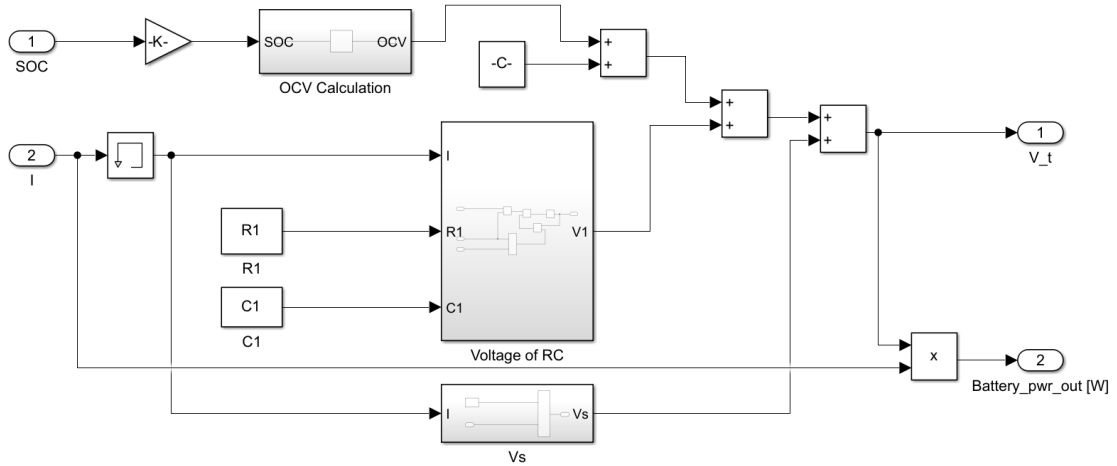


Figure 3.11: Thevenin model

3.3 Parameter estimation

For the estimation of the parameters R_0 , R_1 , C_1 , the matlab tool "Simulink Design Optimisation Toolbox" was used, which allows to follow reference function, entered as input, and the optimal model parameters to be estimated on the basis of that. Using this methodology, the parameters for the various cycles were derived. In particular, the data on reference driving cycles published by Volkswagen are:

- Constant driving: Constant speed cycle at 160 km/h;
- WLTP (Worldwide Harmonised Light Vehicles Test Procedure): defines a globally harmonised standard for determining the levels of pollutants and CO₂ emissions, fuel or energy consumption and range of light electric vehicles;
- FTP (Federal Test Procedure): commonly known as FTP-75 for the city driving cycle, are a series of tests defined by the US Environmental Protection Agency (EPA) to measure tailpipe emissions and fuel economy of passenger cars;
- Urban: Typical urban cycle, where there are low average speeds, lots of acceleration and lots of braking;
- Interurban: Relatively higher average speeds than the urban cycle;
- Highway: Cycle simulating the behaviour of a car on a motorway, with long stretches at high average speeds and higher fuel consumption.

Table 3.1: RC parameters

	$R_0[\Omega]$	$R_1[\Omega]$	$C_1[\text{F}]$
Constant Driving	0.05478	0.05397	3.45939e+04
WLTP	0.07928	0.13684	1.97552e+03
FTP	0.07129	0.03173	6.05655e+02
Urban	0.08940	0.03972	9.98279e+02
Interurban	0.08630	0.00284	4.83648e+02
Highway	0.07343	0.08891	1.29784e+03

A more in-depth description of the different driving cycles is shown in C.

After finding the RC parameters for each cycle, it was found that using the average value for each parameter was a good approximation for characterising the battery. The average RC parameters are:

Table 3.2: RC parameter mean value

	$R_0[\Omega]$	$R_1[\Omega]$	$C_1[\text{F}]$
Mean value	0.07575	0.05900	1470.05

This can be seen in figures 3.12 and 3.13, where the first figure depicts the trend of voltages in an urban cycle. The voltage from the VW data is plotted against that obtained from the developed model. Then the same voltages are compared but changing the RC parameters with the average value of the same. The third tile shows the difference between the voltage obtained from the model with the RC parameters of the respective cycle and the voltage obtained with average RC parameters. It can be seen that in both cases the difference is small, about 1 Volt in the urban case and about 2.5 Volts in the highway case, respectively.

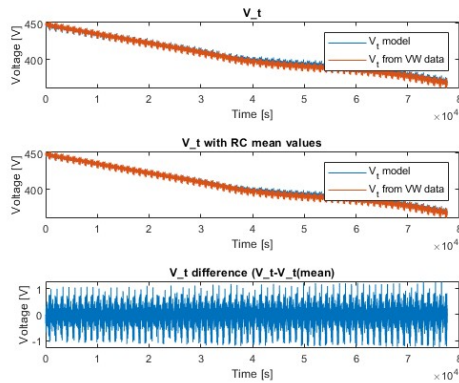


Figure 3.12: URBAN cycle voltage comparison

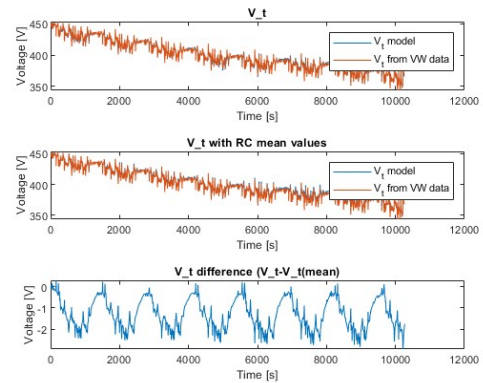


Figure 3.13: HIGHWAY cycle voltage comparison

3.4 Battery degradation factors

LIB aging is the leading cause of change in battery health and life. The internal chemical reaction of the battery is hugely complicated. While explaining the cause of battery aging is not straightforward, a number of studies have been conducted in recent years that have tried to examine and explain the dynamics of battery aging[8]. Path dependence is challenging to take in consideration because of the numerous degradation mechanisms that can occur throughout the life of a cell. It was shown that a multitude of parameters play a key role in degrading a Li-ion cell: depths of discharge (DOD), states of charge, applied currents, temperatures, calendar aging conditions, pulses etc.

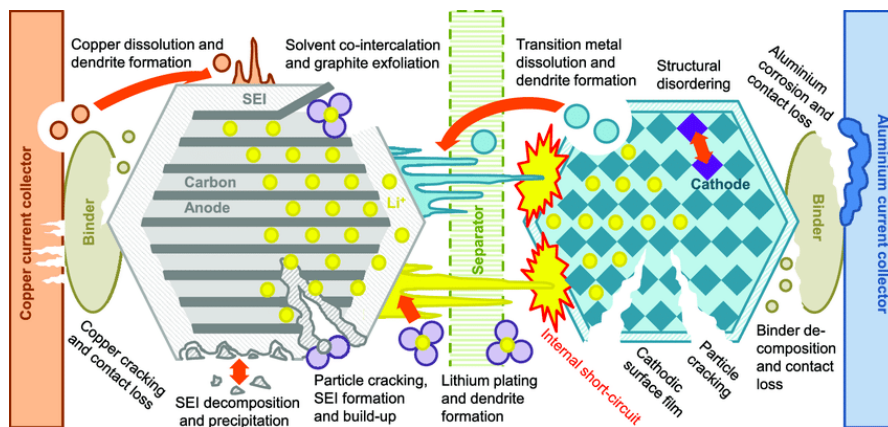


Figure 3.14: Degradation mechanism in Li-ion cells [2]

The operational and storage conditions of lithium-ion batteries can have detrimental effects on their health. The deterioration occurs during charging and discharging, leading to cycle aging, as well as during storage, resulting in calendar aging. In electric vehicles, battery degradation manifests as capacity fade, reducing the achievable range, and impedance rise, diminishing the available power output. Typically, a battery in a battery electric vehicle (BEV) is considered to have reached the end of its life when its available capacity or maximum power under reference conditions has decreased by 20% from its original value. However, capacity loss is usually the primary determining factor, as the battery's initial power capabilities exceed the vehicle's requirements. Modern BEV lithium-ion cells are expected to have a calendar life of five to ten years, depending on the materials used and their management. They should be capable of providing 1000 to 2000 cycles with large state of charge (SOC) variations in electric trucks, and 4000 cycles are anticipated in the near future. This section has a dual purpose: to investigate the causes of lithium-ion battery performance degradation over their lifespan and to explore if such aging can be modeled effectively.

A significant portion of the degradation in current lithium-ion cells with a graphite anode is attributed to chemical reactions occurring at the interface between the anode and the electrolyte. These reactions result in the formation of a solid electrolyte interphase (SEI) on the anode's surface and the consumption of lithium ions, leading to power and capacity fade. Initially, the formation of the SEI during the battery's initial cycles is desirable as it prevents excessive electrolyte decomposition and anode corrosion while still allowing the passage of lithium ions. However, over the battery's lifespan, the SEI film continues to grow and rearrange itself, gradually consuming lithium and further deteriorating the battery's performance. Solid surface layers may also develop at the cathode-electrolyte interface, although they are thinner compared to those formed on the anode. These reactions occurring at the electrode-electrolyte interfaces can impede the flow of lithium ions and generate unwanted gaseous by-products, diminishing the electrolyte's effectiveness. The operating and storage conditions can exacerbate lithium-ion battery degradation mechanisms. High state of charge (SOC), high temperatures, and high charging or discharging rates can accelerate degradation resulting from electrolyte decomposition and SEI formation on the graphite anode.

Large SOC variations during cycling may expedite power fade through SEI growth and potential damage to the cathode materials. Deeper depth of discharge (DOD) can lead to contact losses between certain components on the anode side due to volume variations of the anode materials during cycling. Overcharging the battery beyond the specified cut-off voltage can result in the formation of dendrites on the anode, wasting cyclable lithium and potentially causing severe overheating if the dendrites puncture the separator.

Lithium plating on the anode can occur at low temperatures and high charging rates.

Overcharging can also lead to the loss of active cathode materials. High charging rates in high SOC levels can subject graphite anodes to mechanical degradation such as cracks and fissures. Additionally, certain conditions like high temperatures and low/high SOC levels can result in the dissolution of active cathode materials into the electrolyte, contributing to SEI growth on the anode. The current collectors on the electrodes may also contribute to degradation mechanisms, such as the dissolution of the anode's copper current collector and subsequent dendrite formation when the battery is discharged to low voltage levels. Corrosion of the current collector due to excessively low voltage levels can lead to reduced contact with the anode's materials.

Table 3.3: Overview of lithium-ion battery anode aging mechanisms 3.14

Cause	Effect	Leads to	Reduced by	Enhanced by
Electrolyte decomposition (\rightarrow SEI) (Continuous side reaction at low rate)	Loss of lithium, Impedance rise	Capacity fade, Power fade	Stable SEI, Rate decreases with time	High temperatures, High SOC
Solvent co-intercalation, gas evolution and subsequent cracking formation in particles	Loss of active material (graphite exfoliation), Loss of lithium	Capacity fade	Stable SEI	Overcharge
Decrease of accessible surface area due to continuous SEI growth	Impedance rise	Power fade	Stable SEI	High temperatures, High SOC
Changes in porosity, SEI formation and growth	Impedance rise, Overpotentials	Power fade	External pressure, Stable SEI	High cycling rate, High SOC
Contact loss of active material particles	Loss of active material	Capacity fade	External pressure	High cycling rate, High DOD
Decomposition of binder	Loss of Lithium, Loss of mechanical stability	Capacity fade	Proper binder choice	High SOC, High temperatures
Current collector corrosion	Overpotentials, Impedance rise	Power fade	Current collector pre-treatment	Low SOC
	Inhomogeneous distribution of current and potential	Enhances other aging mechanisms		
Metallic lithium plating and subsequent electrolyte decomposition by metallic lithium	Loss of lithium (Loss of electrolyte)	Capacity fade (power fade)	Narrow potential window	Low temperature, High cycling rate

In summary, lithium-ion battery degradation occurs during storage and cycling due to various chemical and mechanical processes, resulting in capacity fade from the loss of cyclable lithium and active materials, as well as power fade from interface film formation and electrical contact loss. The presence and extent of these degradation mechanisms depend on cell chemistry, storage and operating conditions, and their interactions make degradation prediction and modeling challenging. However, certain recurring factors, such as overcharging, overdischarging, extreme temperatures, high SOC during storage, large DOD, and high charging or discharging rates, can accelerate aging in most lithium-ion batteries. Incorporating these factors into transportation planning problems may be more manageable without expertise in electrochemistry. While some factors can be considered with simple model constraints, others may require more complex degradation models, including storage conditions, charging and discharging rates, temperature, and DOD [9].

3.5 Overview of battery aging models

The requirements and demands that batteries have to meet are constantly increasing. Therefore, effective control and management is crucial for ensuring a safe use of the battery while maintaining the best possible performance. Despite the fact that the diagnosis and prognosis of the State of Health (SOH) is absolutely essential in practical applications, they are not yet effectively implemented in Battery Management Systems (BMS). The main issue hampering the ability of BMSs to accurately track the SoH is the evolution of the voltage response of the cells with aging coupled with the path dependence of the degradation. The latter is a premier issue because it prevents the BMS to use preset look-up tables for SOC recalibration upon aging.

The present state-of-health (SOH) prediction techniques are classified into four distinct groups: model-based approaches, data-driven approaches, hybrid approaches, and alternative approaches. These four categories offer a comprehensive perspective on the current research in SOH prediction. The subsequent sections will provide individual introductions to the first two categories [8].

3.5.1 Model-based method

The categorization of model-based SOH prediction methods can vary among different research studies, resulting in distinct classification criteria. For instance, various terms such as ECM, electrochemical model, mathematical model, life cycle model, physical model, filtering model, mechanism model, and empirical model have been used. In this summary, we group the model-based SOH prediction methods into

three main categories: ECM-based methods, electrochemical model-based methods, and mathematical model-based methods [8].

- **Equivalent Circuit Model (ECM):** The ECM is a model that does not consider the chemical composition inside the battery and corresponding reaction. According to the electrical characteristics of the battery, the basic electronic components and the controlled voltage source are used to construct a model.
- **Electrochemical model-based method:** The internal electrochemical processes in lithium-ion batteries (LIBs) are highly intricate, involving the constant intercalation and de-intercalation of Li ions and the continuous generation and evolution of the solid electrolyte interface (SEI). These phenomena result in changes in the battery's internal mechanisms. The electrochemical model aims to capture the aging mechanisms that contribute to these changes. Among these mechanisms, the SEI-based mechanism model and its corresponding enhanced models, as well as single-factor and multi-factor electrochemical mechanism models, are employed. These models quantitatively describe the microscopic physical and chemical processes occurring within the battery, providing insights from a fundamental perspective. Consequently, the aging mechanism model plays a significant role within the realm of electrochemical model.
- **The mathematical model** encompasses a broad spectrum of approaches. It can be asserted that any model incorporating mathematical equations or other mathematical representations falls within the scope of the mathematical model.

3.5.2 Data-driven method

The data-driven method involves initially constructing a preliminary model and subsequently refining it using extensive data to ensure consistency with the data. In the case of complex electrochemical dynamic systems in lithium-ion batteries (LIBs), model-based approaches are often intricate and challenging to implement. On the other hand, the data-driven method does not take into account the specific electrochemical reactions and failure mechanisms occurring within LIBs. Consequently, data-driven prediction methods have emerged as a prominent area of research [8].

- **Artificial intelligence-based method:** The AI-based method employs artificial neural networks (ANN), support vector machines (SVM), relevance vector machines (RVM), and other intelligent algorithms, such as machine learning theory, grey theory, and fuzzy algorithms, to establish a mapping relationship between characteristic parameters and the degradation lifetime of lithium-ion

batteries (LIBs). Subsequently, these methods are used to extrapolate the estimated state of health (SOH) and remaining useful life (RUL).

- **Filtering-based method:** The filtering-based method is widely employed for robust estimation purposes. It typically involves two steps: prediction and correction. This method constructs a state-space model by formulating a state equation and considers parameters such as internal resistance and capacity as state variables that characterize the state of health (SOH) of the battery. Through dynamic tracking and prediction, the filtering algorithm iteratively solves the model to estimate the health.
- **Time series-based method:** In simple terms, the time series-based method predicts future trends based on past patterns. The fundamental time series-based prediction methods include the simple sequential mean method, weighted sequential mean method, moving average method, weighted moving average method, and others. Typically, these methods assign varying weights to data points within a moving window based on their influence, and then calculate the average value to forecast future values.

3.5.3 Hybrid methods

Hybrid methods, as the name implies, are approaches that combine multiple distinct methods. Currently, hybrid methods typically involve combining methods of the same type or methods of different types. Furthermore, there are combinations that incorporate optimization algorithms and other techniques, which generally improve performance by optimizing model parameters and thresholds.

3.6 Battery aging model

There is currently a wide range of methods available for State of Health (SOH) prediction. Numerous researchers assert the superiority of their respective methods. The accuracies of these methods are consistently high, which can lead to confusion in discussions. However, it is important to note that each proposed SOH prediction method has its specific scope of application, and superior results can be achieved under certain circumstances. Moreover, the complexity and operational characteristics of each method vary, which can impact their practical implementation. Therefore, it is essential to evaluate these SOH prediction methods in order to comprehend their scope of application and complexity. Such evaluations serve as a valuable reference for real-world implementation and future research endeavors. A semi-empirical mathematical model developed by Prof. Onori and published in [10] will be used in this thesis. In her work, the damage accumulation model used

to predict battery cycle life is calibrated on battery aging data obtained from a charge sustaining HEV and includes SOC, temperature and current rate dependence.

The battery's ability to resist aging is proportional to its nominal C-rate. The model used in this thesis is based on an energy oriented battery and since in the case of a fuel cell electric vehicle there is a more power oriented battery, of which we have no data. We have therefore chosen to use a normalized C-rate to simulate its behavior. Specifically, the ratio of the maximum C-rate of a battery in a bus solution to the C-rate of the VW battery was used. Thus the input current, when battery aging is analyzed, was divided by this value, which takes the value of $k = 3.78$.

Aging in batteries is a non-reversible phenomenon resulting from unwanted chemical reactions occurring within the battery. There are two primary forms of battery aging: calendar aging and cycle-life aging [11], but we will only consider the cycle aging.

Severity factors are commonly used to describe the factors that contribute to battery aging. In the context of hybrid electric vehicle (HEV) applications, these severity factors typically include state of charge (SOC), C-rate, which is defined as the ratio of battery current (I) to actual capacity (Q), and battery internal temperature. The capacity loss model used in this scenario is established based on a complete dependency on severity factors. This dependency is captured through a severity factor function denoted as σ_{funct} . The following relationship exists between σ_{funct} and Q_{loss} :

$$Q_{loss}(SOC, I_c, \theta, Ah) = \sigma_{funct}(SOC, I_c, \theta) \cdot Ah^z \quad (3.8)$$

where Q_{loss} is the percent capacity loss, defined as $Q_{loss} = (1 - Q/Q_0) \cdot 100$, where Q_0 is the initial capacity in [Ah]; z is an empirical power exponent; and Ah is the accumulated ampere-hour throughput of the battery, given by $Ah = \int_0^t \frac{|I|}{3600} d\tau$. SOC is expressed as a fraction, I_c is in [1/h] and θ is in [$^{\circ}C$]. The severity factor function assumes the following form:

$$\sigma_{funct}(SOC, I_c, \theta) = (\alpha \cdot SOC + \beta) \cdot \exp\left(\frac{-Ea + \eta|I_c|}{R_g(273.15 + \theta)}\right) \quad (3.9)$$

where α , β e η are model parameters, Ea is the activation energy in [J/mol] and R_g is the universal gas constant in [$J/mol/K$].

In Simulink, the battery model seen above was adapted so that the formula just presented could be carried out. The Simulink model is presented below in 3.15.

In the "Aging model" block, the formulation seen above is represented in 3.9, where the values of α and β , are reported in 3.4; for η , a value equal to 152.5

results in the best fitting. The value of z is 0.57 and the temperature, θ , is assumed constant with a reference value of 20 °C.

The electric battery model seen in 3.9 was implemented with some modifications. The operation is always the same. It receives as input the initial SOC and the current profile so that the current SOC can be calculated, which will then be the input into the aging formula block as the α and β parameters depend on the SOC. The aim of this model is to cycle the behaviour of the battery until the EOL is reached, that is the 20% State of Health (SOH) is lost.

In a first analysis, to see how good the formulation was with the model data, it was decided to use the parameters provided by Prof. Onori's article [10]. Subsequently, the parameter estimation tool was used and the reference parameters for an Urban and a Highway guide were found. These parameters follow the trend of the reference driving cycles very well, but due to the exponential trend, it was not possible to derive reference values that are valid for every cycle.

Table 3.4: Optimal values of α and β

	α	β
SOC [%] < 45	2896.6	7411.2
SOC [%] \geq 45	2694.5	6022.2

Table 3.5: Optimal values for Urban cycles

	URBAN
α	-2.67065
β	2.27585e+03
η	-0.60664
z	0.62392

Table 3.6: Optimal values for Highway cycles

	HIGHWAY
α	-2.7965
β	1.4422e+04
η	-0.11927
z	0.48722

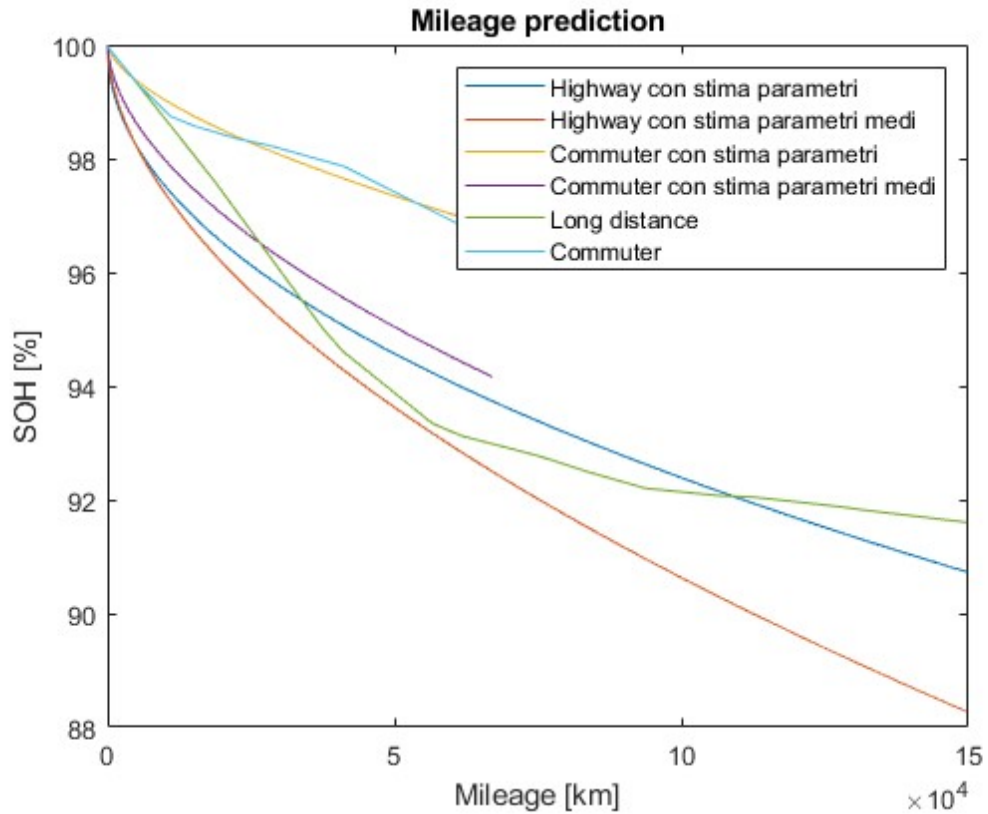


Figure 3.16: Aging comparison for different aging parameters

In 3.16, a more concise representation of the trend of the various curves is shown, obtained using the reference parameters present in tables 3.5 and 3.6 respectively for Urban and Highway. These two curves ("Commuter con stima parametri, Highway con stima parametri") were then compared with the reference ones ("Commuter, Long distance") taken from [7] and two other curves ("Commuter con stima parametri medi, Highway con stima parametri medi") obtained using the mean of the parameters present in the tables 3.5 and 3.6.

It is possible to notice how aging, when using average parameters, is more pronounced compared to the optimal values assigned previously.

It was therefore possible to assume that through the use of the aging parameters presented in [10], it is possible to obtain a trend more similar to the desired one and it is shown in fig 3.17. Downstream of this, in the next chapters it will be taken for granted that, in the case of battery aging analysis, the parameters present in 3.4 are used.

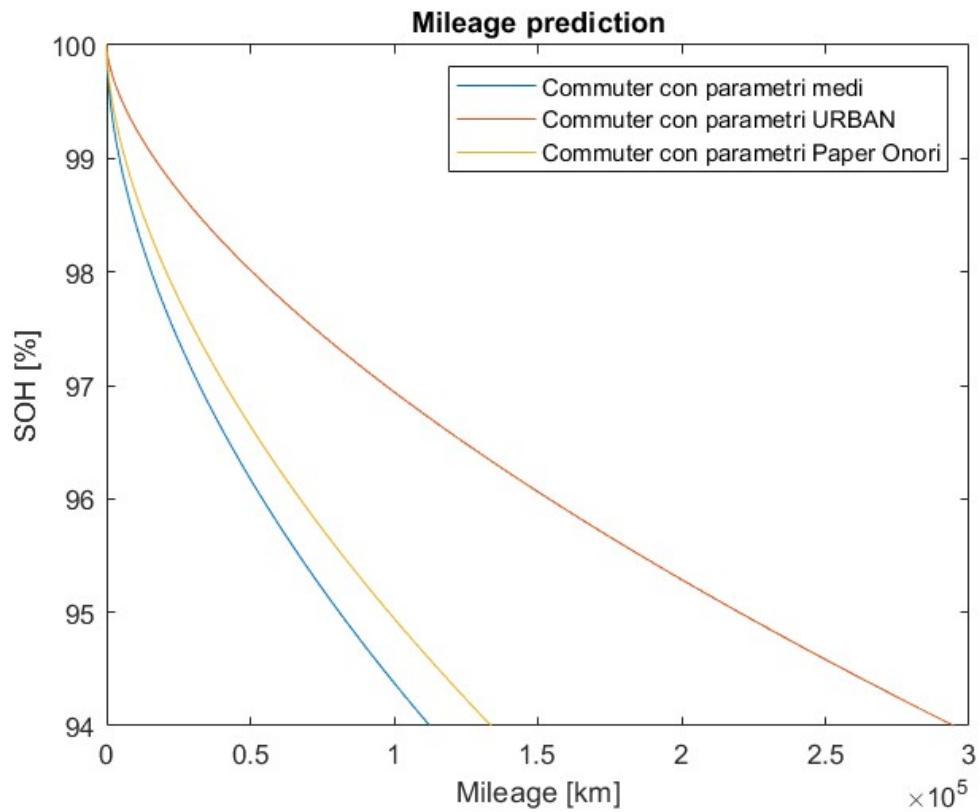


Figure 3.17: Aging comparison for Urban Cycle and different aging parameters

In figure 3.15, the Smulink model with which the battery aging simulation is performed is shown. The model was built in such a way that the electrical behavior of a single cycle could be cycled until the battery EOL is reached. In figure 3.18, the equation 3.9 is implemented, which will have as output the percentage of capacity lost by the battery

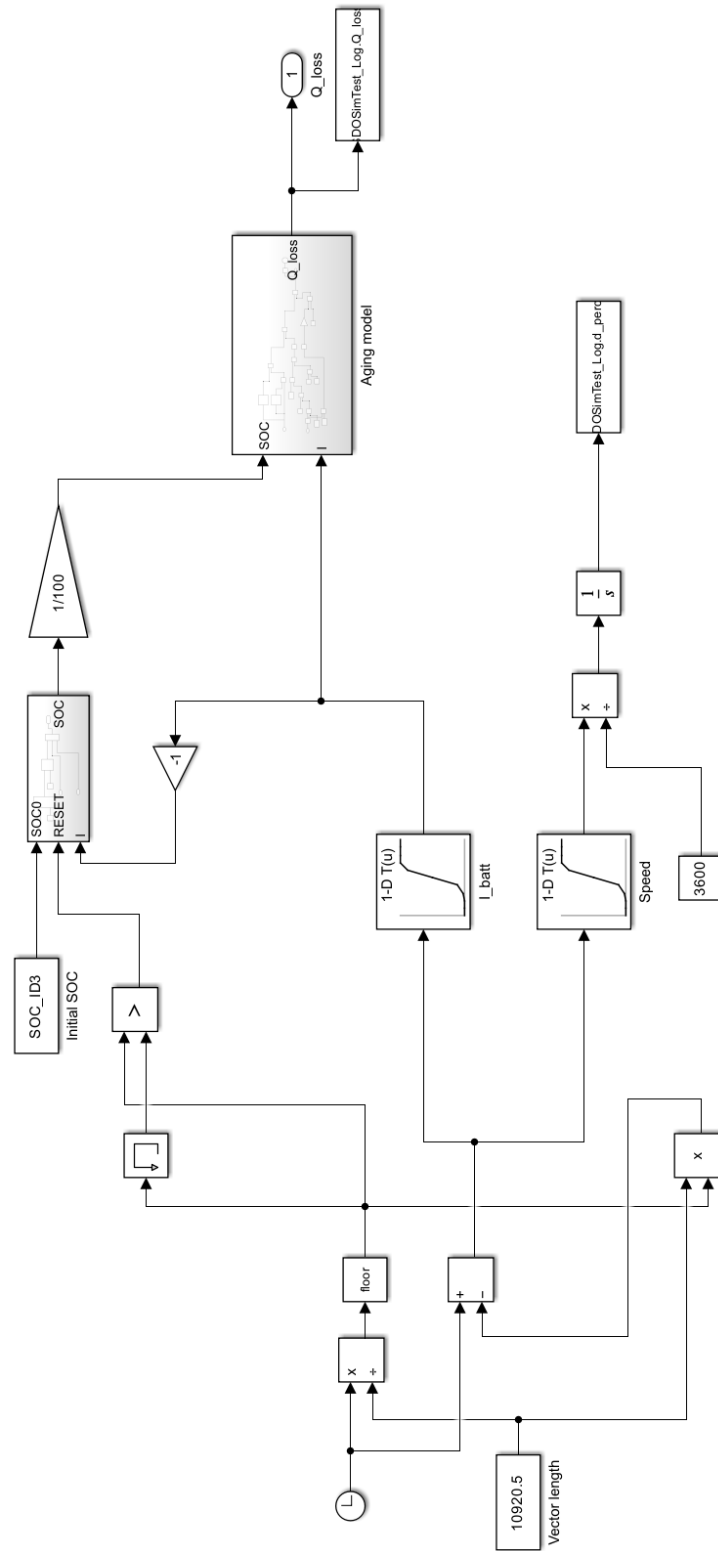


Figure 3.15: Complete aging model

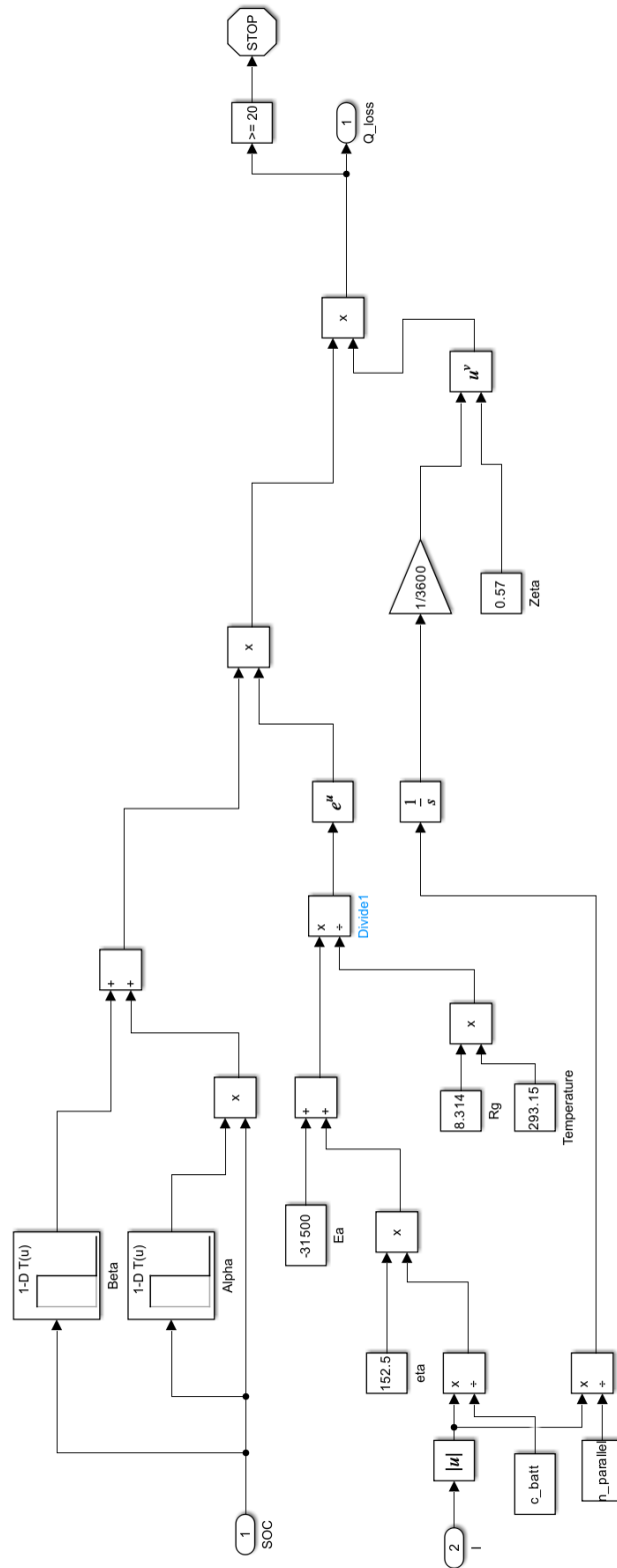


Figure 3.18: Battery aging formula represented in Simulink

Chapter 4

Fuel Cell

A fuel cell is an electrochemical device that converts the chemical energy of a fuel, often hydrogen, and an oxidizing agent, typically oxygen, into electricity through a series of redox reactions. Unlike most batteries, fuel cells require a continuous supply of fuel and oxygen (usually from the air) to sustain the chemical reaction, whereas batteries typically rely on existing substances within the battery for chemical energy. Fuel cells have the capability to generate electricity continuously as long as there is a supply of fuel and oxygen.

The initial development of fuel cells dates back to 1838 when Sir William Grove invented the first fuel cells. Nearly a century later, the hydrogen-oxygen fuel cell was invented by Francis Thomas Bacon in 1932, marking the beginning of commercial fuel cell applications. The alkaline fuel cell, also known as the Bacon fuel cell, has been utilized in NASA's space programs since the mid-1960s to generate power for satellites and space capsules. Since then, fuel cells have found applications in various fields. They are used for primary and backup power in commercial, industrial, and residential buildings, as well as in remote or inaccessible areas. Fuel cells also power vehicles such as forklifts, cars, buses, trains, boats, motorcycles, and submarines. As shown in 4.1, fuel cells have attracted the scientific community, leading to an increased number of publications over the years.

Fuel cells exhibit various types, yet they operate on a fundamental principle. They consist of three adjacent components: the anode, the electrolyte, and the cathode. At the interfaces of these segments, two chemical reactions take place. As a result, fuel is consumed, and either water or carbon dioxide is generated, while concurrently producing an electric current that can be utilized to power electrical devices, commonly known as the load.

In the anode, a catalyst initiates the ionization of the fuel, typically hydrogen, separating it into a positively charged ion and a negatively charged electron. The

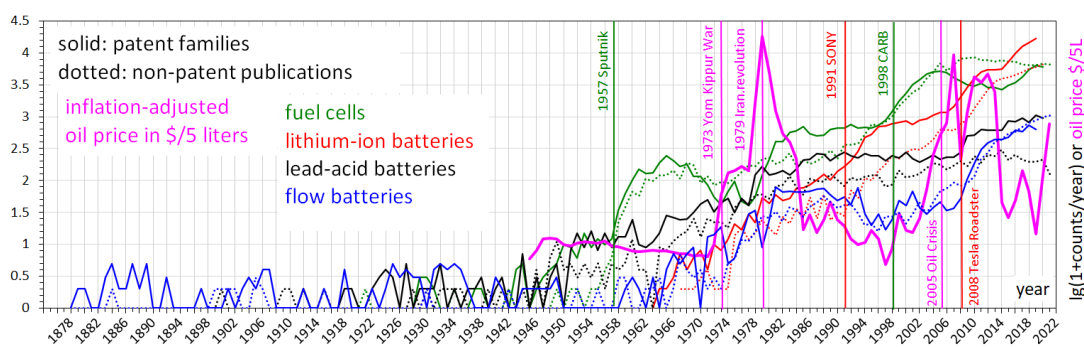


Figure 4.1: Electrochemical power sources by year price comparison

electrolyte is a specially designed substance that allows ions to pass through while preventing the movement of electrons. The released electrons travel through a wire, generating an electric current. Meanwhile, the ions move through the electrolyte toward the cathode. Upon reaching the cathode, the ions reunite with the electrons and react with a third substance, often oxygen, resulting in the formation of water or carbon dioxide. Key elements in fuel cell design encompass:

- The electrolyte material, which typically determines the fuel cell type and can be composed of various substances like potassium hydroxide, salt carbonates, or phosphoric acid.
- The fuel used, with hydrogen being the most common choice.
- The anode catalyst, typically employing fine platinum powder to break down the fuel into electrons and ions.
- The cathode catalyst, often utilizing nickel, which converts ions into waste compounds, commonly resulting in water.
- Gas diffusion layers engineered to resist oxidation.

Voltage decreases as current increases due to several factors:

- Activation loss.
- Ohmic loss, referring to the voltage drop caused by the resistance of cell components and interconnections.
- Mass transport loss, occurring when reactants deplete at catalyst sites under high loads, leading to a rapid voltage decline.

To deliver the desired energy output, fuel cells can be connected in series to achieve higher voltage or in parallel to enable a higher current supply. This configuration, known as a fuel cell stack, allows for increased cell surface area, thereby accommodating higher current from each cell.

4.1 Proton-exchange membrane fuel cell (PEMFC)

Proton Exchange Membrane Fuel Cells (PEMFCs) have attracted considerable attention as environmentally friendly and highly efficient devices for energy conversion in recent years. It is being recognized as a leading choice for future power generation due to its numerous benefits such as high efficiency in converting energy, lower emissions of greenhouse gases, flexibility in fuel usage, and compact design.

PEMFCs are electrochemical devices that enable the direct conversion of chemical energy from a fuel source, typically hydrogen, and an oxidizing agent, such as oxygen, into electricity through redox reactions.

PEMFCs offer numerous compelling advantages. Firstly, they exhibit remarkably high conversion efficiency, allowing for effective transformation of chemical energy into electricity. Moreover, PEMFCs significantly contribute to the reduction of greenhouse gas emissions, promoting a cleaner and more sustainable energy generation process. Their versatility in fuel usage and compact design further enhance their appeal, making them suitable for various applications, including residential, commercial, and electric vehicles.

Despite their numerous advantages, PEMFCs do face certain limitations. One primary challenge is their dependence on a continuous supply of fuel and oxygen, necessitating the development of robust hydrogen production and delivery infrastructure. Furthermore, the high cost associated with catalyst materials, such as platinum, poses a significant barrier to the widespread adoption of PEMFCs. Additionally, ensuring the durability and stability of the proton exchange membrane is crucial, as it has a limited lifespan and can be vulnerable to degradation from fuel contaminants or environmental factors.

To fully realize the potential of PEMFCs as a sustainable energy solution, continuous research and technological advancements are necessary to address these challenges.

4.2 Characteristics and working principles

A Proton Exchange Membrane Fuel Cell (PEMFC) is an electrochemical device that converts the chemical energy released from the electrochemical reaction between hydrogen and oxygen into electrical energy, rather than relying on the direct combustion of hydrogen and oxygen gases for thermal energy production.

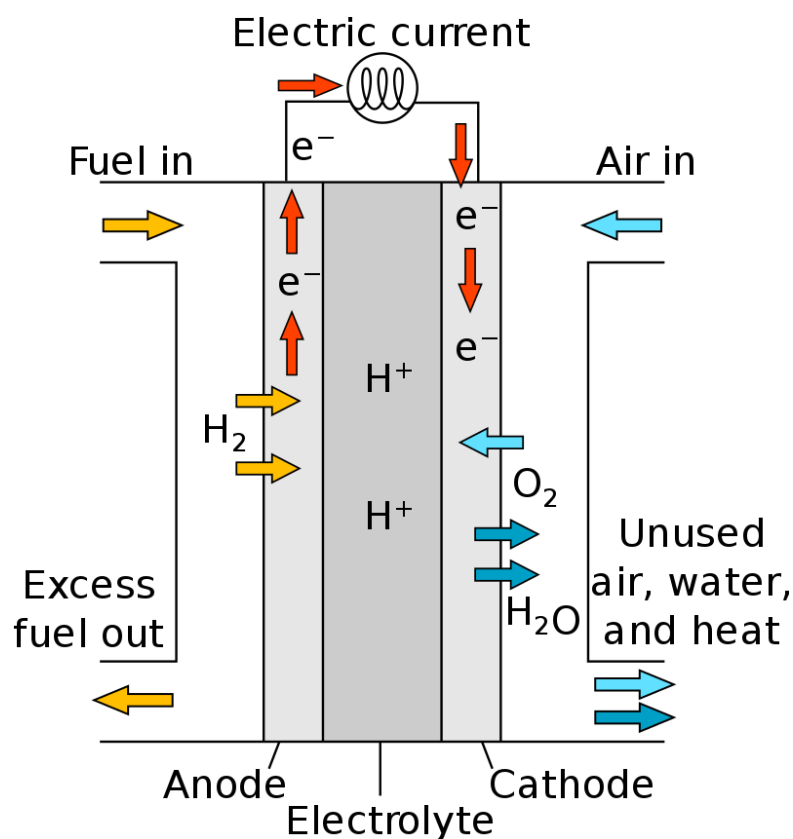


Figure 4.2: Components of Fuel Cell

Hydrogen gas is delivered to the anode side of the Membrane Electrode Assembly (MEA), where it undergoes catalytic oxidation, splitting into protons (H⁺) and electrons (e⁻), as shown in 4.2. This oxidation reaction, known as the hydrogen oxidation reaction (HOR), can be represented as follows:

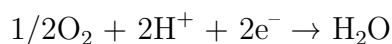
At the anode:



The generated protons migrate through the polymer electrolyte membrane to

the cathode side. Simultaneously, the electrons travel through an external circuit, creating the electric current output of the fuel cell. On the cathode side, an oxygen stream is supplied to the MEA. Oxygen molecules react with the migrating protons and electrons at the cathode to form water molecules. This reduction reaction, known as the oxygen reduction reaction (ORR), can be represented as follows:

At the cathode:



The overall reaction combines the hydrogen and oxygen reactions, resulting in the formation of water:



It's important to note that the given potentials are with respect to the standard hydrogen electrode. The reversible nature of the reaction demonstrates the recombination of hydrogen protons, electrons, and oxygen molecules to produce water.

belsec:Aging

4.3 FC degradation factors

The PEMFC, which is an open reactor, can be significantly influenced by numerous factors, impacting its operational performance. These factors include various operating conditions (such as suboptimal air compressor control strategies, elevated stack temperatures, insufficient humidity), the natural degradation of materials (such as membrane deterioration, degradation of carbon electrodes, catalytic decline), and mechanical stresses (such as electrode leaks or losses in contact). These unpredictable circumstances contribute to the progressive decline in the performance of the fuel cell system over time (aging), consequently hindering its widespread adoption and deployment.

There are some major failure modes of different components of PEM fuel cells. In a typical PEM fuel cell configuration, the membrane is positioned between two catalyzed electrodes. Its primary functions include facilitating proton transport, supporting the catalyst layers at the anode and cathode, and most importantly, separating the oxidizing (air) and reducing (hydrogen) environments on the respective sides. Consequently, an excellent membrane must meet stringent requirements such as high protonic conductivity, gas permeability, thermal and chemical stability, among others. Numerous research studies have focused on understanding the

mechanisms behind membrane degradation and failure in fuel cell environments. However, the unsatisfactory durability and reliability of membranes remain critical obstacles to the commercialization of PEM fuel cells.

4.3.1 Membrane degradation mechanisms

Membrane degradation can be classified into three categories: mechanical, thermal, and chemical/electrochemical [12].

- Mechanical degradation of the membrane: Mechanical degradation can cause early-life failures due to defects like perforations, cracks, tears, or pinholes. These defects may arise from inherent issues in the membrane or improper fabrication processes during the membrane electrode assembly (MEA). Local regions exposed to excessive or non-uniform mechanical stresses, such as the interface between lands and channels in the flow field or sealing edges, are particularly susceptible to small perforations or tears. Additionally, operational factors such as non-humidification, low humidification, and relative humidity cycling can lead to dimensional changes that negatively impact mechanical durability. Migration and accumulation of catalysts, as well as seal decomposition into the membrane, have adverse effects on membrane conductivity and mechanical strength, significantly reducing ductility. The presence of local pinholes and perforations in the membrane can result in the crossover of reactant gases into their respective reverse electrodes. This can lead to highly exothermic reactions on the catalyst surface, generating localized hotspots. Overall, the understanding of membrane degradation mechanisms is crucial for addressing issues related to durability and reliability in PEM fuel cells.
- Thermal degradation of the membrane: Thermal degradation of the membrane is another important aspect to consider. In order to ensure adequate hydration of PFSA (Perfluorosulfonic Acid) membranes, the preferred operating temperature range for PEM fuel cells is typically between 60 to 80 degrees Celsius. Conventional PFSA membranes are susceptible to significant degradation at high temperatures due to the glass transition temperatures of PFSA polymers, which occur around 80 degrees Celsius. However, achieving rapid startup, stable performance, and easy operation at subfreezing temperatures is crucial for the commercialization of fuel cell technologies in applications such as vehicles and portable power supplies. On the other hand, recent efforts have been focused on developing PEM fuel cells that can operate at temperatures above 100 degrees Celsius to enhance electrochemical kinetics. It should be noted that the protonic conductivity of the membrane decreases significantly as the water content decreases, especially when the fuel cell is operated at

high temperatures and under low humidity conditions. Balancing the thermal requirements with the hydration needs of the membrane is essential to maintain optimal performance and prevent thermal degradation in PEM fuel cells. For fuel cells to achieve successful commercialization in automotive and portable applications, it is crucial for membranes to exhibit resistance to freezing temperatures and thermal cycling. Membranes should be capable of withstanding subfreezing conditions and fluctuating thermal environments without compromising their performance and durability. This requirement is essential to ensure the reliable operation and long-term viability of fuel cells in real-world applications.

- Chemical/electrochemical degradation of the membrane: Studies have demonstrated that the rates of hydrogen and air crossover to the opposite sides of the membrane are relatively slow and result in only a marginal 1-3% decrease in fuel cell efficiency. However, it is important to note that the highly exothermic reaction between hydrogen (H_2) and oxygen (O_2) can potentially lead to the formation of pinholes in the membrane, resulting in the degradation of the Membrane Electrode Assembly (MEA) and causing significant issues. Furthermore, the chemical reactions occurring on the anode and cathode catalysts can generate peroxide ($HO\bullet$) and hydroperoxide ($HOO\bullet$) radicals, which are commonly believed to contribute to chemical degradation of the membrane and catalysts. These radicals are responsible for initiating chemical attacks that can impair the performance of both the membrane and the catalysts. Further investigation has also revealed that the generation of these radicals as well as the chemical degradation of the membrane is accelerated when the fuel cell is operated under open circuit voltage (OCV) and low humidity conditions. In relation to the chemical and electrochemical degradation of the membrane, significant emphasis has been placed on the development of membranes that exhibit exceptional chemical stability against peroxy radicals. This specific area of research has garnered significant attention as scientists and engineers seek to enhance the durability and longevity of membranes in fuel cell applications.

Mechanical degradation can cause early-life failures due to defects like perforations, cracks, tears, or pinholes. These defects may arise from inherent issues in the membrane or improper fabrication processes during the membrane electrode assembly (MEA). Local regions exposed to excessive or non-uniform mechanical stresses, such as the interface between lands and channels in the flow field or sealing edges, are particularly susceptible to small perforations or tears. Additionally, operational factors such as non-humidification, low humidification, and relative humidity cycling can lead to dimensional changes that negatively impact mechanical durability.

Migration and accumulation of catalysts, as well as seal decomposition into the membrane, have adverse effects on membrane conductivity and mechanical strength, significantly reducing ductility. The presence of local pinholes and perforations in the membrane can result in the crossover of reactant gases into their respective reverse electrodes. This can lead to highly exothermic reactions on the catalyst surface, generating localized hotspots.

Overall, the understanding of membrane degradation mechanisms is crucial for addressing issues related to durability and reliability in PEM fuel cells.

4.3.2 Electrocatalyst and catalyst layer

Significant research has been devoted to thoroughly investigating the degradation mechanism of Pt (Platinum) catalysts during prolonged operation. Initially, a pristine Pt catalyst can be tainted by impurities originating from the input reactants or the fuel cell system. Additionally, the catalyst's efficiency may decline due to the aggregation or movement of Pt particles on the carbon support, detachment and dissolution of Pt into the electrolyte, and corrosion of the carbon support. Several mechanisms have been proposed to explain the enlargement of catalyst particle size during PEM fuel cell operation:

- The growth of particles can occur through Ostwald ripening, where small Pt particles dissolve in the ionomer phase and redeposit on the surface of larger particles. This phenomenon leads to particle growth. Moreover, dissolved Pt species can diffuse into the ionomer phase and precipitate in the membrane by reducing Pt ions with crossover hydrogen from the anode side. This process significantly reduces membrane stability and conductivity.
- Platinum particles can agglomerate on the carbon support at the nanometer scale due to random cluster-to-cluster collisions, resulting in a log-normal distribution of particle sizes with a peak at smaller sizes and a tail towards larger sizes.
- Particle growth can also occur at the atomic scale through the minimization of cluster Gibbs free energy. In this case, the particle size distribution is characterized by a peak at larger sizes and a tail towards smaller sizes. However, there is still no consensus on the dominant mechanism responsible for catalyst particle growth. The coarsening of the catalyst, caused by particle movement and coalescence on the carbon support, leads to a decrease in the catalyst active surface area.
- Lastly, the formation of metal oxides at the anode or cathode side likely contributes to an increase in particle sizes, ultimately resulting in a decline in catalyst activity.

Recent studies have proposed and successfully implemented various strategies to enhance the durability of catalysts. Firstly, the degradation of catalysts is influenced by the operating conditions of the fuel cell. Pt dissolution from the carbon support is less likely to occur at lower electrode potentials, making Pt catalysts more stable at the anode than at the cathode. Secondly, the corrosion of the carbon support due to fuel starvation can be mitigated by improving water retention on the anode. This can be achieved through modifications to the PTFE and/or ionomer, incorporating water-blocking components like graphite, and utilizing more efficient catalysts for water electrolysis. Thirdly, Pt-alloy catalysts, such as PtCo and Pt-Cr-Ni, have demonstrated improved activity and stability compared to pure Pt catalysts.

4.3.3 Gas diffusion layer

The gas diffusion layer (GDL) in fuel cells is subject to degradation mechanisms that can affect the performance and durability of the cell. The primary degradation mechanisms include carbon corrosion, hydrophobicity loss, and pore blockage.

Carbon corrosion occurs when the GDL comes into contact with reactive species, such as radicals and peroxides, produced during fuel cell operation. This corrosion leads to the loss of carbon material from the GDL, reducing its electrical conductivity and overall performance.

Loss of hydrophobicity refers to the decrease in the GDL's ability to repel water. Over time, the GDL can become wetter, resulting in increased flooding of the catalyst layer and reduced reactant transport. This can lead to performance degradation and cell failure.

Pore blockage occurs when contaminants, such as particles and electrolyte by-products, accumulate in the GDL pores, restricting gas and liquid transport. This can impede reactant distribution, reduce mass transfer, and hinder the cell's performance.

To mitigate these degradation mechanisms, various strategies have been explored, including the development of corrosion-resistant carbon materials, hydrophobic coatings, and advanced GDL designs with improved pore structure and permeability [12].

4.3.4 Bipolar plate

The bipolar plates in fuel cells are prone to degradation mechanisms that can impact the long-term performance and durability of the cell. The primary degradation mechanisms include corrosion, fouling, and mechanical damage.

Corrosion is a significant concern for bipolar plates, especially those made of metal. The corrosive environment within the fuel cell, combined with the presence of contaminants and aggressive species, can lead to the degradation of the plate

material. Corrosion can result in the loss of plate thickness, formation of pits, and changes in surface morphology, ultimately affecting the electrical conductivity and structural integrity of the plates.

Fouling refers to the accumulation of impurities, such as carbonaceous deposits, catalyst residues, and minerals, on the surface of the bipolar plates. This fouling layer can obstruct the flow of reactants and products, reduce gas diffusion, and create localized concentration gradients, leading to performance losses.

Mechanical damage can occur due to various factors, including thermal stresses, vibrations, and improper assembly. These factors can result in cracks, delamination, or deformation of the bipolar plates, affecting their mechanical stability and sealing integrity.

To mitigate these degradation mechanisms, researchers have explored different strategies. These include using corrosion-resistant materials, applying protective coatings, implementing effective cleaning methods to remove fouling, and optimizing the design and manufacturing processes to enhance the mechanical robustness of the plates.

By understanding and addressing these degradation mechanisms, efforts are aimed at improving the durability, reliability, and overall performance of fuel cell systems [12].

4.3.5 Sealing gasket

The sealing gaskets in fuel cells are susceptible to degradation mechanisms that can impact the performance and durability of the cell. The primary degradation mechanisms include compression set, chemical degradation, and thermal degradation.

Compression set refers to the loss of elastic properties and the permanent deformation of the gasket material over time. The constant compression and relaxation cycles experienced during fuel cell operation can lead to reduced sealing effectiveness, resulting in gas and liquid leakage. This can impair the cell's performance and compromise its overall efficiency.

Chemical degradation occurs when the gasket material comes into contact with aggressive species, such as fuel cell electrolytes or reactants. Exposure to these chemicals can cause chemical reactions that degrade the gasket material, leading to its deterioration and loss of sealing capability. This degradation mechanism can be accelerated under high-temperature and high-humidity conditions.

Thermal degradation refers to the degradation of the gasket material due to prolonged exposure to high temperatures during fuel cell operation. The high operating temperatures can cause thermal stress, leading to material degradation, loss of elasticity, and reduced sealing effectiveness. Thermal degradation can also be exacerbated by thermal cycling, which involves repeated heating and cooling of the gasket material.

To mitigate these degradation mechanisms, researchers have explored different approaches. These include selecting gasket materials with high resistance to compression set and chemical attack, optimizing the design and geometry of the gasket, implementing effective sealing techniques, and employing thermal management strategies to minimize thermal stress and temperature fluctuations [12].

4.4 FC aging model

[13] studied the influence of typical operating conditions on the lifetime of a vehicular fuel cell. In this article, the lifetime dependence of fuel cells is defined as a function of:

- Start-stop condition: one event was assumed at the beginning of the cycle and equal to 5s;
- Open-circuit/idle and low power condition: The load demand to the FC is below 8.5 kW (10% Max power);
- High-power load condition: the gross power demand to the FC is above 73kW (90% Max power);
- Load-changing condition: it is equal to the difference between the cycle duration and the sum of the other working conditions.

Therefore, a fuel cell vehicle's driving condition and the total degradation rate can be simulated as the sum of these four typical operating conditions:

$$d = \{d_1, d_2, d_3, d_4\} \quad (4.1)$$

$$g = \{g_1, g_2, g_3, g_4\} \quad (4.2)$$

where, d_i and g_i stand for the voltage degradation rate and the weight coefficients of the load-changing condition, start-stop condition, idle condition and high-power load condition, respectively. A higher weight coefficient for an operating condition makes it more likely that the fuel cell is operated under this condition.

The weight factors are calculated as the ratio between each working condition and the cycle duration and are presented in table 4.2. The degradation coefficients are set equal to the reference values from literature and are presented in table 4.1.

This leads to the definition of the equation of residual life:

$$Residual \ lifetime[h] = \frac{\Delta V}{k \cdot V(d_1g_1 + d_2g_2 + d_3g_3 + d_4g_4)} \quad (4.3)$$

where ΔV represents the permitted voltage variation magnitude from the current time to the point where the voltage declines by 10%, V is the voltage at the current time and k is an environmental factor that is primarily related to the air pressure and input quantity of gas.

Table 4.1: Degradation coefficients

Operating condition	Load-changing	Start-stop	Idle	High-power
Degradation rate	0.00332	0.00196	0.00126	0.00147

So to summarise, equation 4.3 analyses fuel cell aging in real time using the current voltage measurement and weighing the other parameters according to the operating condition. Unfortunately, no data on the current voltage of the fuel cell were available. So a $\frac{\Delta V}{V}$ value of 0.1 was assumed. As a value of k , the reference value from the article was initially used, i.e. $k=1.8$.

Table 4.2: Weight factors values

	Load changing	Start-stop	Idle	High power
SORT 1 [s]	476.47	5	451.93	0
%	0.51046	0.00535	0.48417	0
SORT 2 [s]	386.26	5	348.54	0
%	0.52211	0.00675	0.47112	0
Braunschweig [s]	1430	5	245.53	0
%	0.8297	0.002901	0.14246	0

Plugging all the values just presented into the formula, a residual lifetime similar to that exhibited in [13] was found. Specifically, the resulting residual lifetime in Sort 1 is:

$$Residual\ lifetime[h] = 2399.484652 \quad (4.4)$$

very close to that referenced in the article.

In terms of the latest technology, the residual lifetime for a fuel cell bus is approximately at least 10,000 hours. We can therefore modify the parameter k , seen earlier in the equation 4.3, that allows us to achieve the target operating lifetime. By imposing the operating life to 10,000 hours in the SORT 1 cycle, we can obtain a value of k , which is equal to 0.43190. With this value of k , we can then determine the operating lives for the other two cycles: 9,893.29 hours for SORT 2 and 7,267.02 hours for Braunschweig.

More conclusions on these results will be given in the dedicated chapter 6.

Chapter 5

Bus model in Simulink

This chapter will comment on the complete Simulink model of the bus, thus including both battery and fuel cell. The model is represented in 5.1. It presents the desired speed as the only initial input, and the role of all the blocks in the figure is to model the FC+battery behavior to follow the path. In particular, the model in 5.1 includes these blocks:

- Driver;
- Vehicle controller;
- Electric motor;
- Vehicle dynamic;
- DC-link;
- Battery;
- Energy manager logic;
- Fuel Cell;

Now, in order, we will go into the details of each of these blocks

5.1 Driver block

A hypothetical driver is simulated in this block. Specifically, this is done in the "Driver Model" block with reference to the figure 5.2. Through a PID controller 5.3, which has as input the difference between the desired speed and the current speed, the driver behavior trying to follow the path is simulated. There are two control signals at the output, one regarding acceleration (if the signal value is between 0 and 1) and the other for braking (if the signal value is between -1 and 0).

5.2 Vehicle controller model

Referring to the figure 5.4, eight input signals can be seen: acceleration and braking signal, the current speed, rotation speed of the omega motor, the state of charge, and finally the current power output from the fuel cell and the power limits of the fuel cell. Through these inputs, the goal is to obtain a torque output command, one for acceleration and one for braking. The signal output will be in $Nm(Newton \cdot meter)$.

5.3 Vehicle dynamic

The brake torque signal output of the previous block will be the input for the vehicle dynamics block. Together with the motor torque they are the inputs for the vehicle longitudinal dynamics equation. Vehicle dynamics can be expressed by the vehicle equation:

$$F_{inertia}(t) = M_{veh} \frac{dv_{veh}}{dt}(t) = F_{trac}(t) - F_{aero}(t) - F_{roll}(t) - F_{grade}(t) \quad (5.1)$$

where:

- M_{eqv} is the equivalent mass of the vehicle;
- V_{veh} is the longitudinal vehicle speed;
- $F_{inertia}$ is the inertia force;
- F_{trac} Tractive force = Engine brake force;
- F_{roll} Rolling resistance. Is defined as:

$$F_{roll}(t) = c_{roll}(v_{veh}) \cdot M_{veh} \cdot g \cos\theta(t) \quad (5.2)$$

where c_{roll} is the rolling coefficient, which is function of the vehicle speed, M_{veh} is the vehicle mass, g is the gravitational acceleration and θ is the road slope;

- F_{aero} Aerodynamic resistance. Can be approximated as:

$$F_{aero}(t) = \frac{1}{2} \rho_{air} \cdot A_f \cdot C_d \cdot v_{veh}^2(t) \quad (5.3)$$

where ρ_{air} is the air density, A_f is the frontal area, C_d is the drag coefficient and V_{veh} is the vehicle speed;

- F_{grade} Resistance force due to road slope:

$$F_{grade}(t) = M_{veh} \cdot g \cdot \sin\theta(t) \quad (5.4)$$

5.4 DC-link

In the DC-link 5.7 a power balance is made between the power required by the electric motor and the power output by the fuel cell. The result will be the power required, at any moment, from the battery. In this model, in fact, the fuel cell is used as if it were a sort of battery charger. The power of the auxiliary components (such as: lights, air conditioning, etc.) has also been included in the dc-link. An auxiliary power of 7.5 kW was assumed

5.5 Battery

We have already talked about this block in chapter 2, at the input it receives the required power, at the output of the DC-link, and by dividing it with the current voltage we obtain the current in Ampere. With the input current, the current SOC is calculated as well as the voltages, and therefore the electrical behavior of the battery, through the Thevenin model. This block is shown in figure 5.8.

5.6 Energy manager logic

In this block, as shown in 5.9, a fuel cell switch on logic is implemented based on the current SOC. As mentioned before, the fuel cell in this model is used as a battery charger. This behavior is implemented in this block, in detail it works that when the SOC drops below a certain threshold, 85% of charge, the fuel cell turns on. The more discharged the battery, the more power the fuel cell will deliver. This logic is shown in figure 5.10

5.7 Fuel cell

Figure 5.11 shows the block for characterizing the fuel cell. This characterization takes place through the use of a look-up table which shows the efficiency of the fuel cell with respect to the required power. So based on the required power, which is the input of the block, you get the real power delivered by the fuel cell.

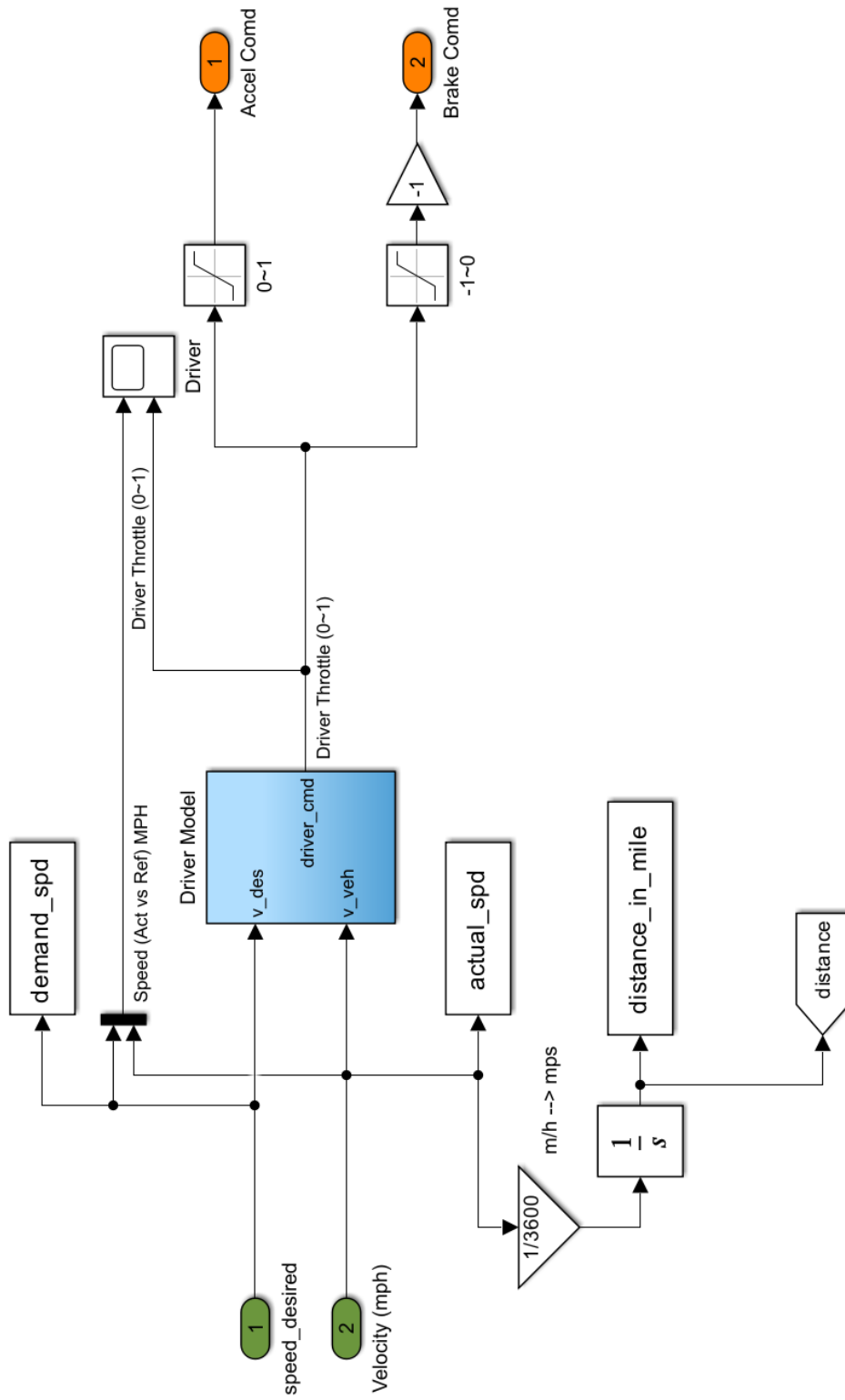


Figure 5.2: Driver

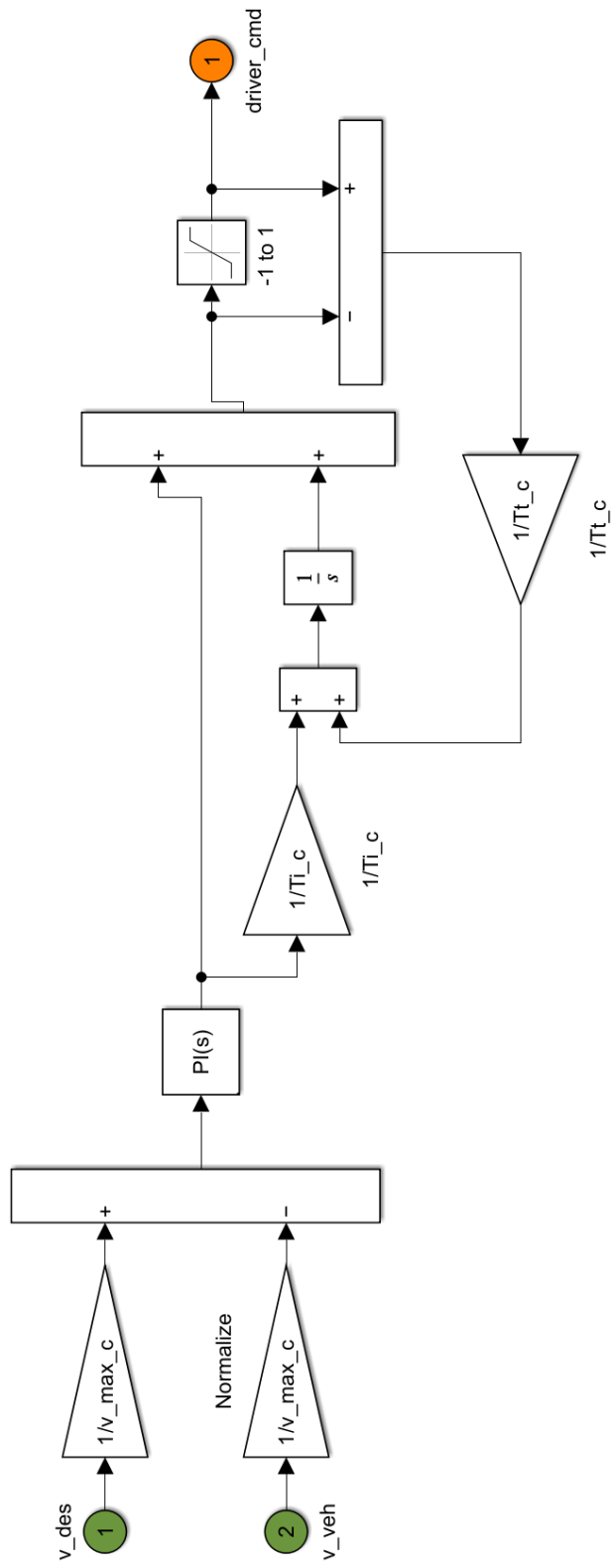


Figure 5.3: PID model

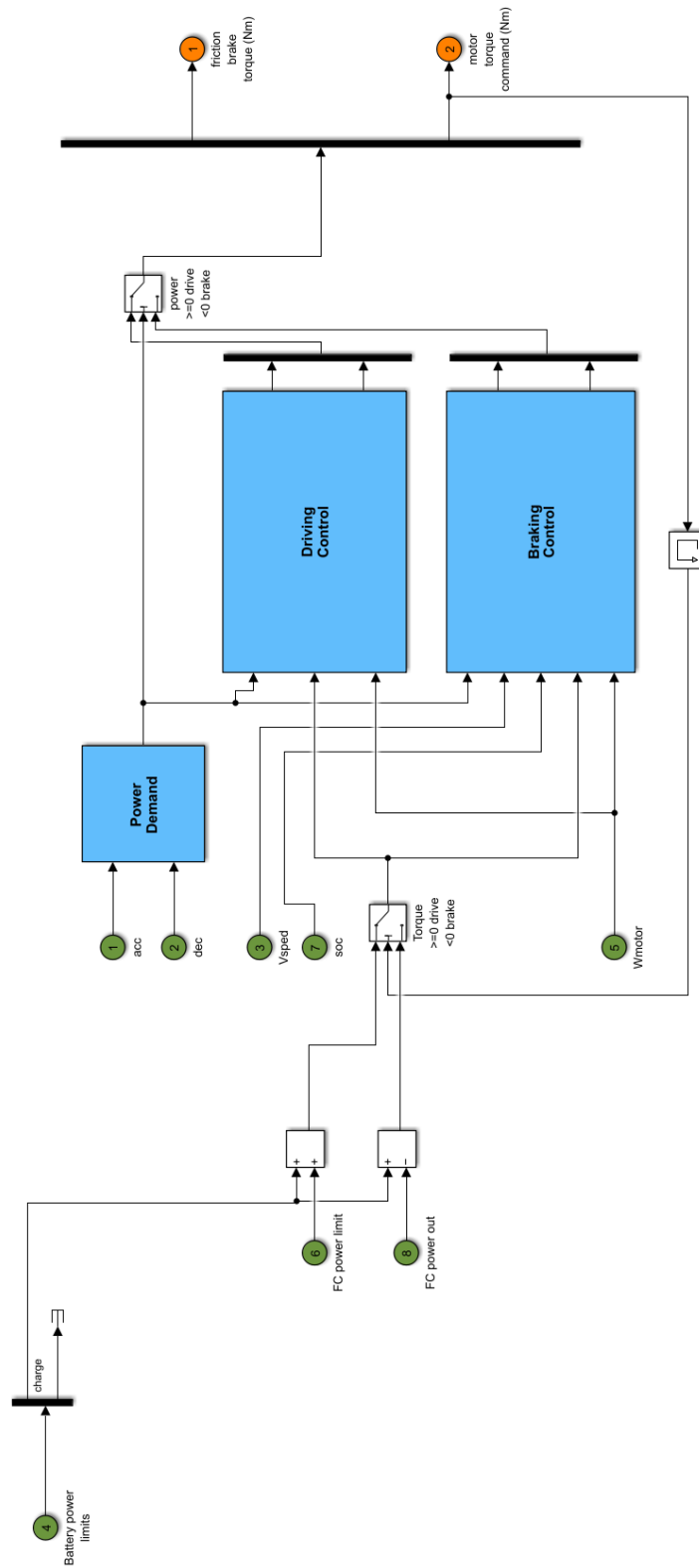


Figure 5.4: Vehicle controller

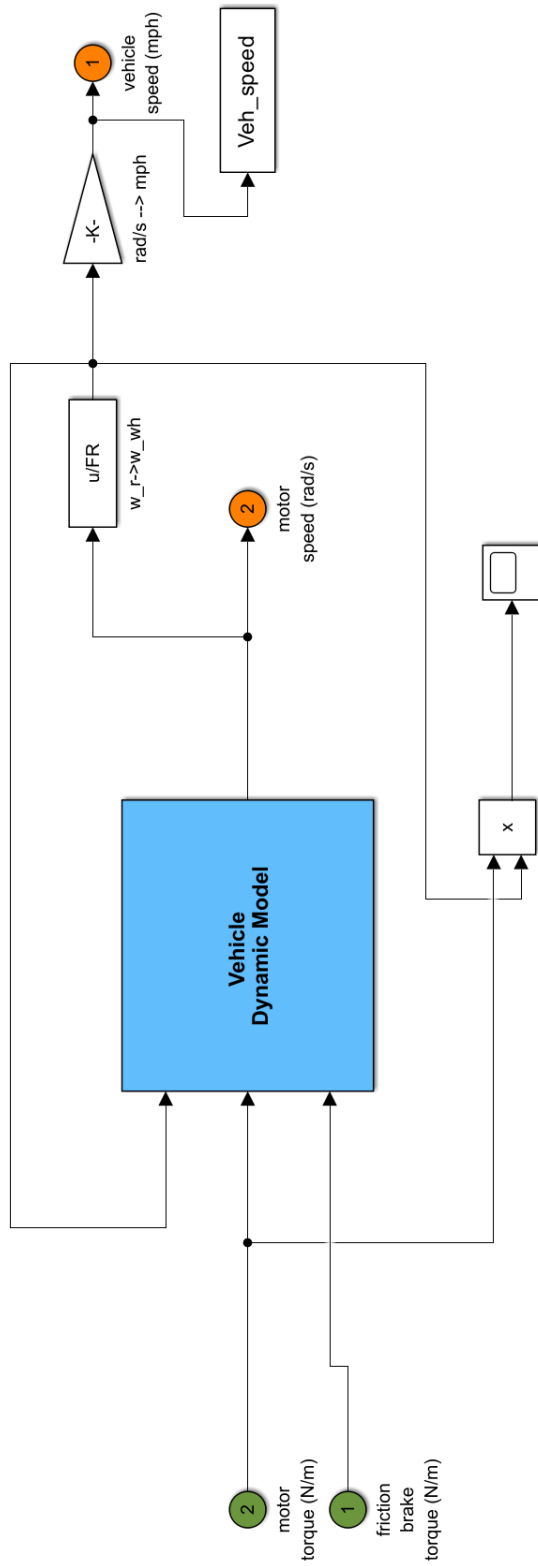


Figure 5.5: Vehicle dynamic model

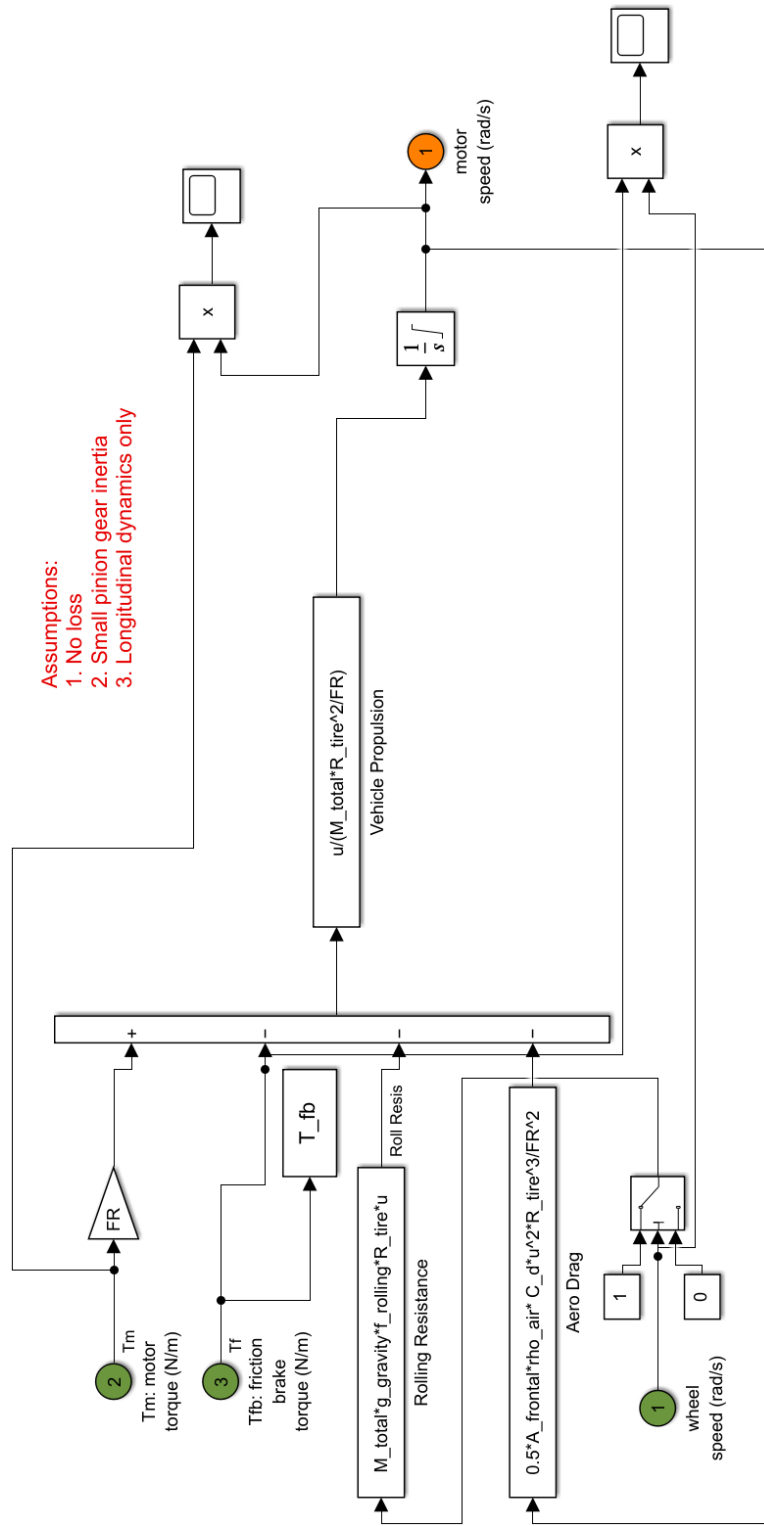


Figure 5.6: Longitudinal vehicle dynamics

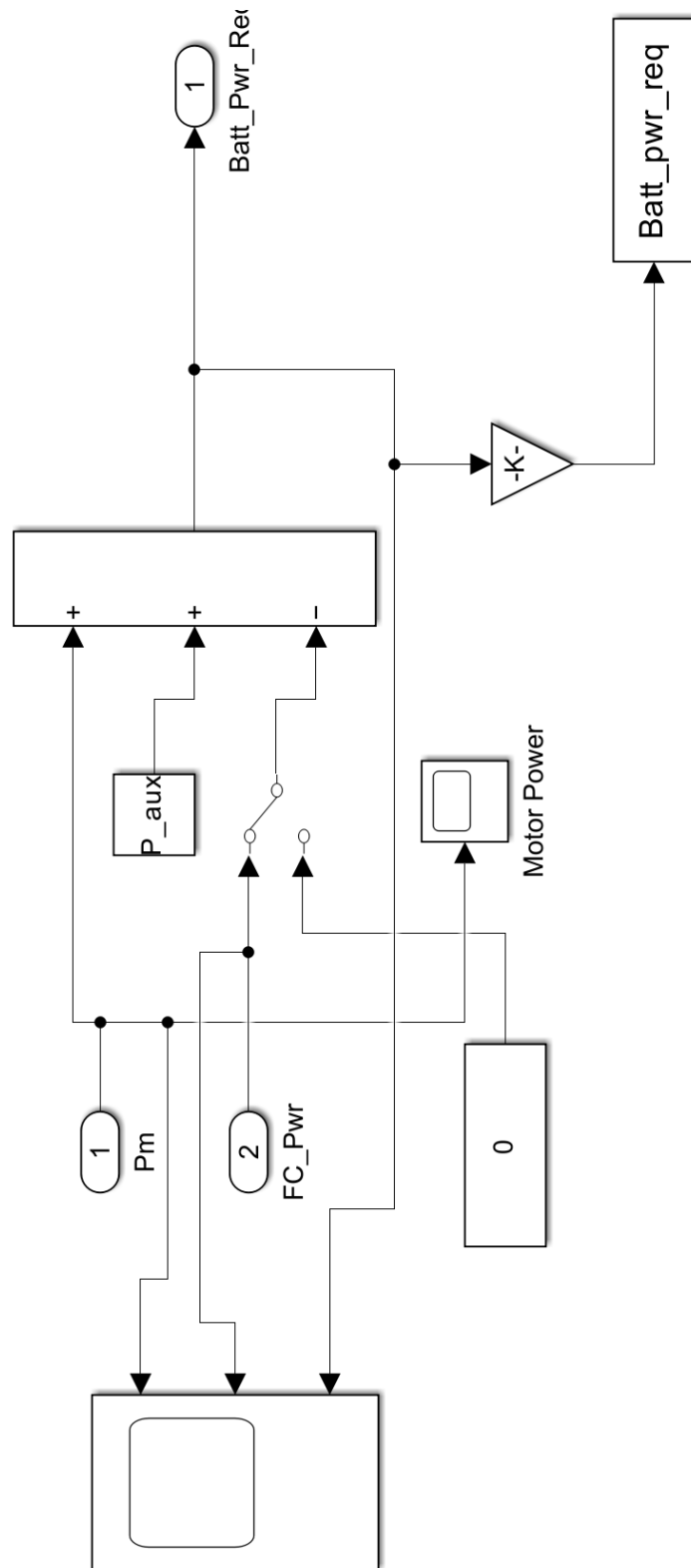


Figure 5.7: DC-link model

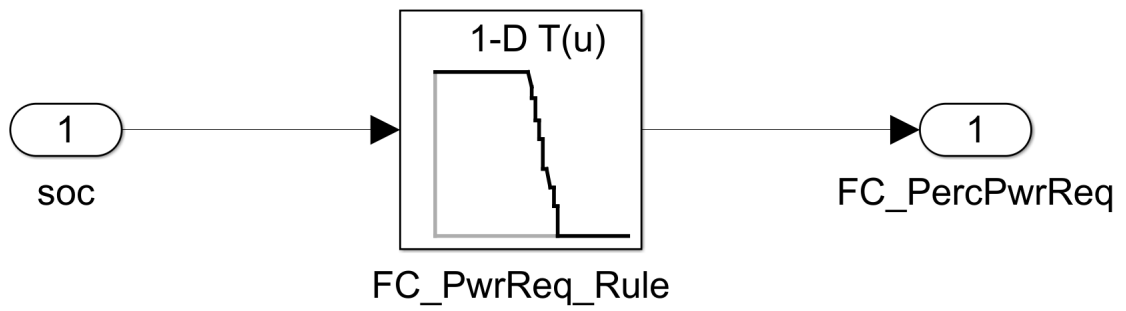


Figure 5.9: Energy manager logic model

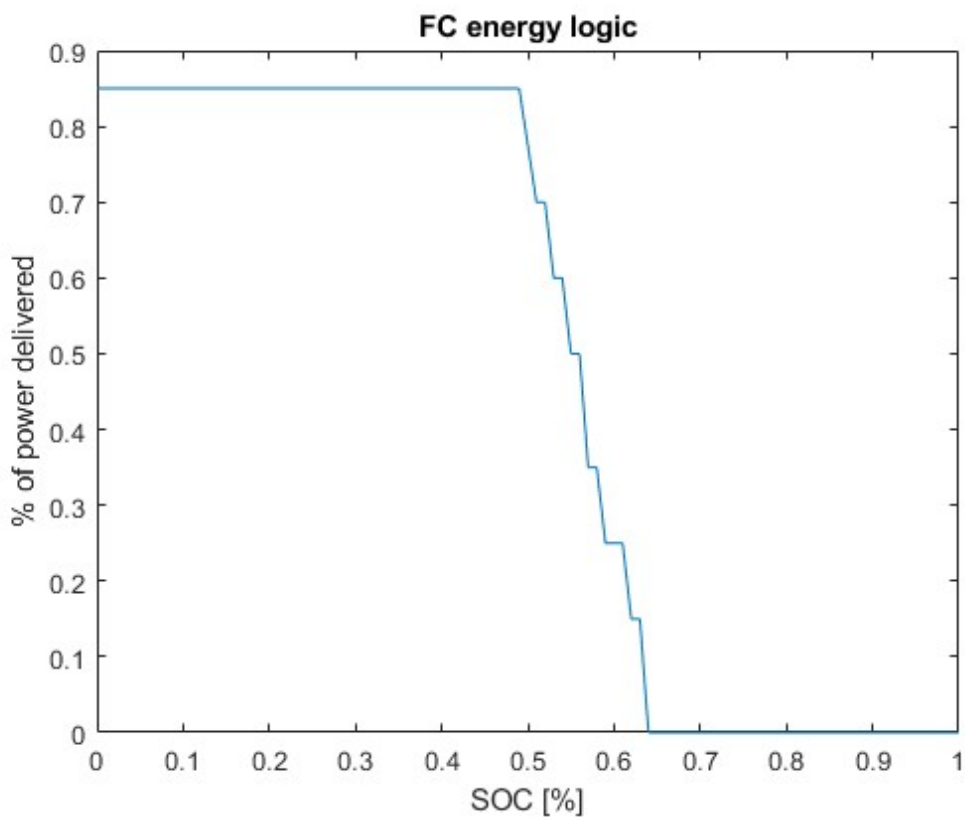


Figure 5.10: FC logic

Chapter 6

Results

This chapter shows, through plots made on Matlab, an overview of the results obtained in this thesis. In particular, the comparison between the requested speed and the current speed of the vehicle, the electrical behavior of the battery, the balance of power to the electric motor and the aging of the battery. Each drive cycle was run on matlab until conditions stabilized. In this way, problems deriving from the beginning of the cycle are avoided, in which the condition for recharging the fuel cell in relation to the SOC must still be satisfied.

6.1 SORT 1

The SORT 1 driving cycle consists of various driving phases that mimic urban driving conditions, including frequent stops, accelerations, and decelerations. These characteristics are designed to reflect the typical traffic patterns and driving behavior observed in urban areas.

The SORT 1 driving cycle emphasizes low-speed driving, with an average speed significantly lower than that of other driving cycles. This phase includes frequent stops at traffic lights, junctions, and intersections, as well as slow accelerations and decelerations.

The SORT 1 driving cycle also includes an idling phase to account for the time heavy-duty vehicles spend stationary with their engines running, such as during traffic congestion or while loading and unloading goods. This phase assesses the emissions generated during prolonged idling periods.

The total duration of the SORT 1 driving cycle is typically around 20 minutes. This duration is selected to capture the typical driving patterns and provide a comprehensive assessment of heavy-duty vehicle emissions and fuel consumption under low-speed urban conditions.

In figure 6.4, is possible to notice how the vehicle is able to follow the trace of the requested speed.

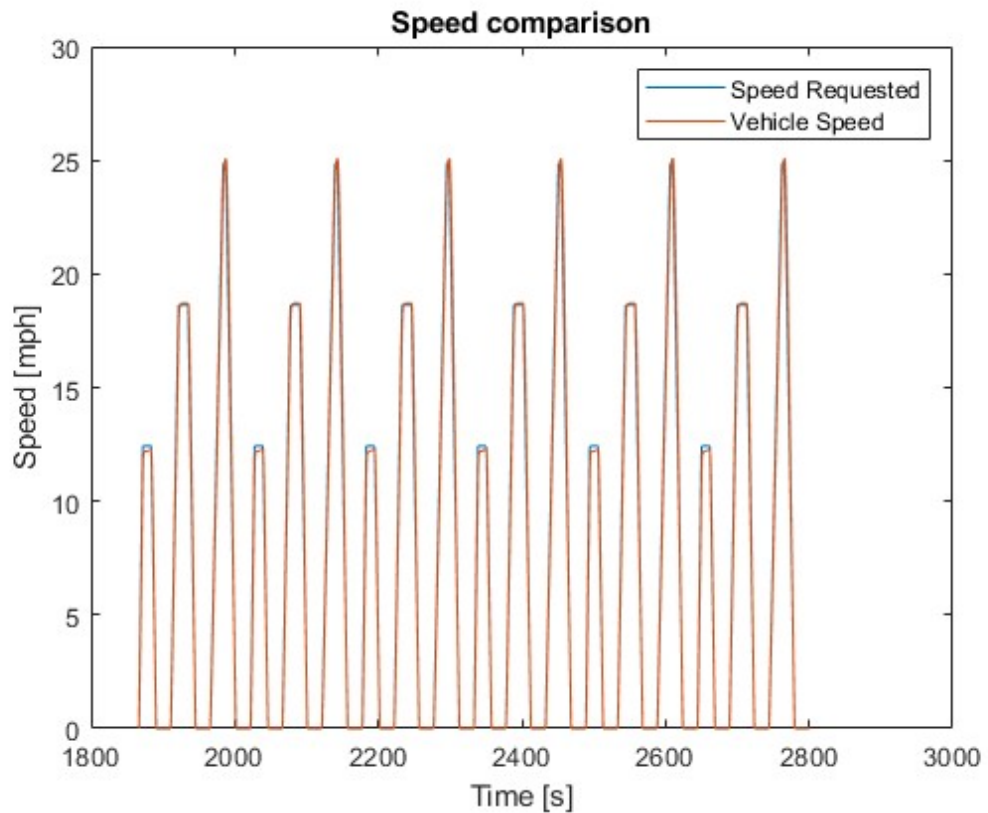


Figure 6.1: Speed requested vs Vehicle speed - SORT 1

This figure 6.2 shows the power balance of the electric motor. In particular, the first tile shows the net power to the electric motor, the second tile shows the power delivered by the battery and the third tile shows the output power from the fuel cell. From the power output of the battery can be observed regeneration during braking and how power consumption follows the trend of the vehicle. From the fuel cell it can be seen that it is used at low power as the battery is not under much strain.

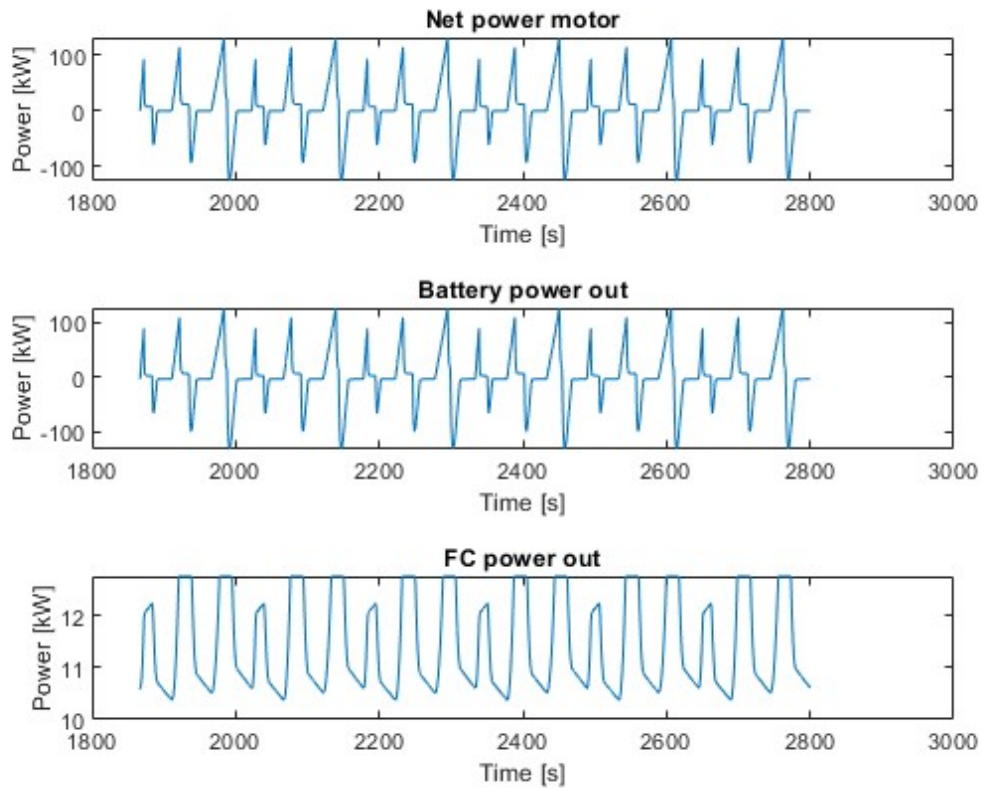


Figure 6.2: Power balance - SORT 1 (sign convention: +discharge -charge)

6.3 shows the parameters of the electrical characterization of the battery: voltage, current, power and state of charge (SOC). It is also possible to notice how the SOC has a fairly zig-zag pattern as it is charged by the fuel cell and the charge is a function of the (SOC) with reference to the switch on logic present in figure 5.10.

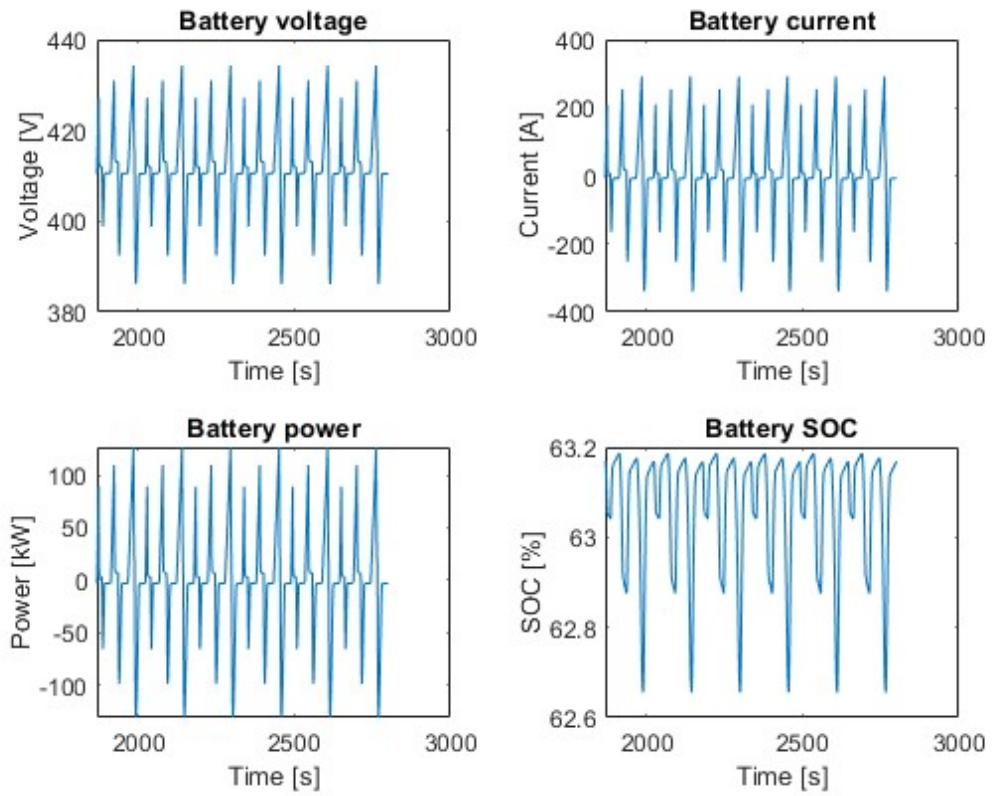


Figure 6.3: Battery parameters - SORT 1 (sign convention: +discharge -charge)

6.2 SORT 2

Cycle sort 2 is a mix between an urban and a suburban cycle. The main difference with sort 1 is a higher average speed

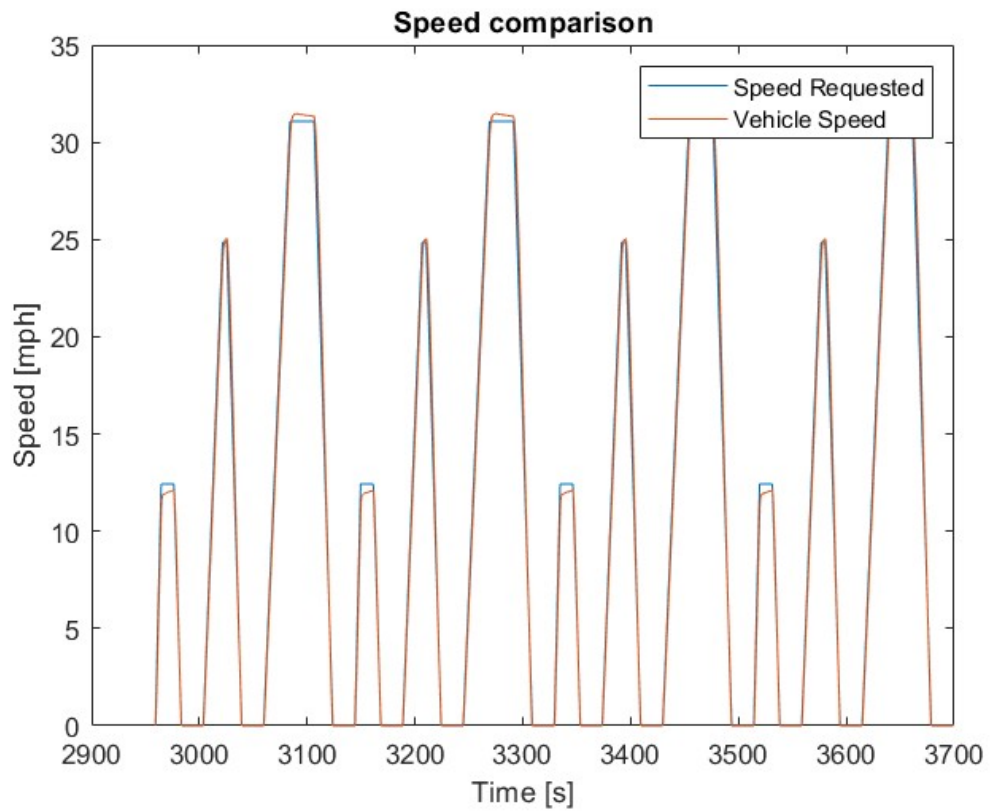


Figure 6.4: Speed requested vs Vehicle speed - SORT 2

The only difference to note in 6.5 respect 6.2 is that there are higher battery power and a slightly higher fuel cell output power.

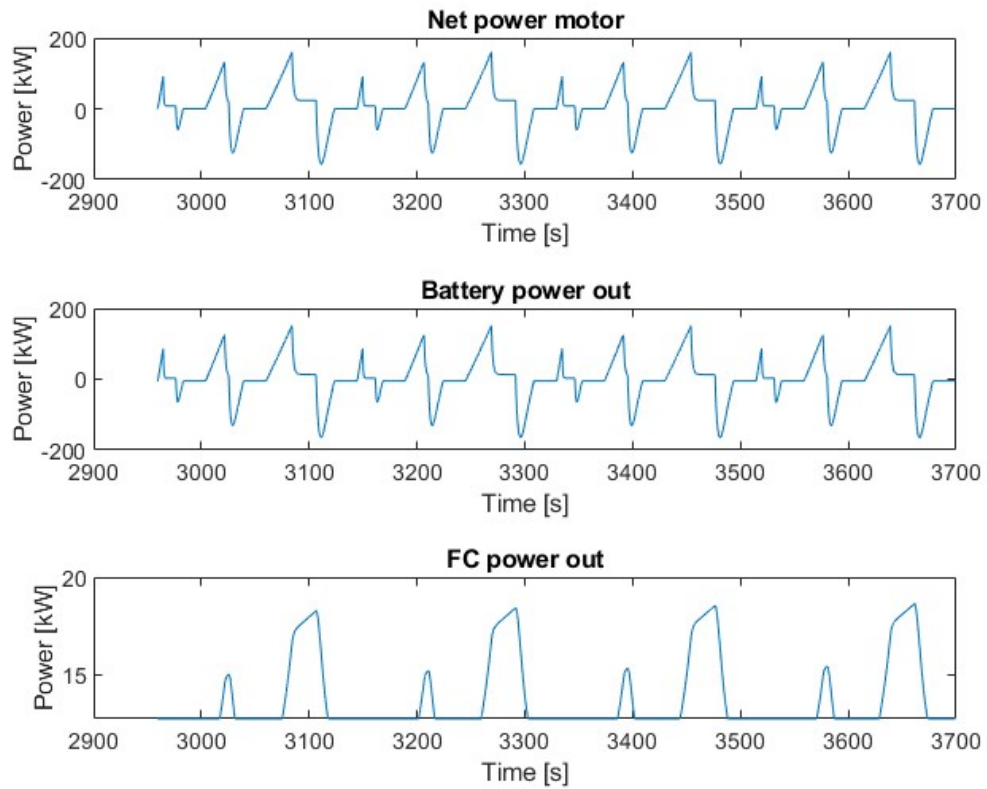


Figure 6.5: Power balance - SORT 2 (sign convention: +discharge -charge)

Nothing to highlight as the electrical parameters do not differ much from the trend seen in SORT 1.

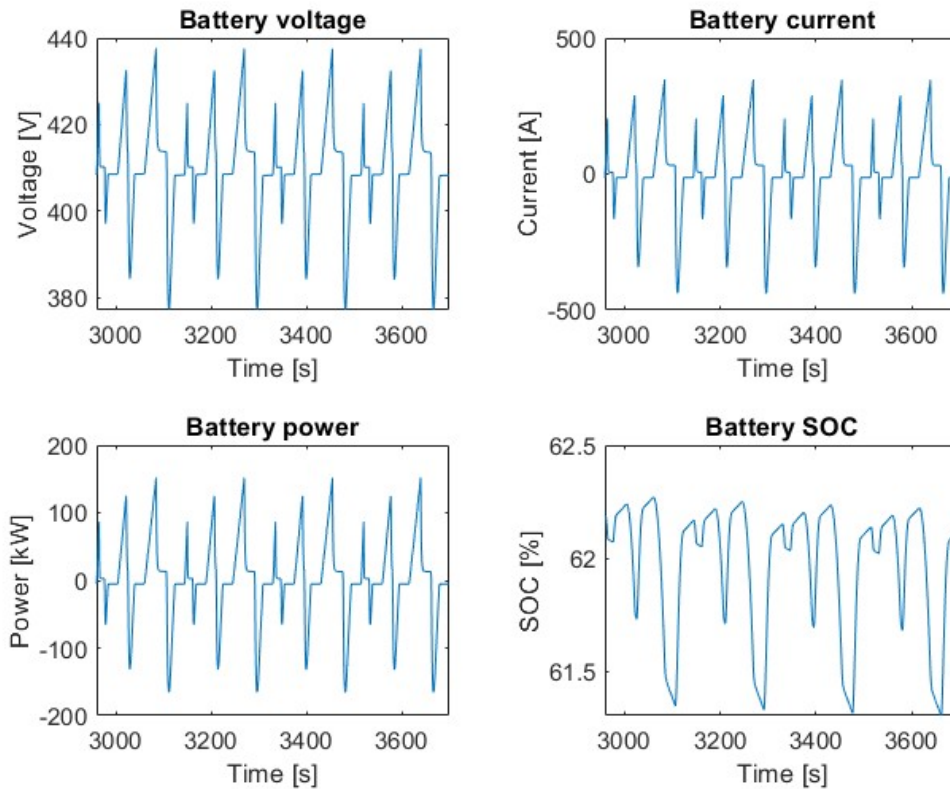


Figure 6.6: Battery parameters - SORT 2 (sign convention: +discharge -charge)

6.3 Braunschweig

The Braunschweig driving cycle is designed to represent typical urban driving conditions encountered in cities. It aims to provide a realistic simulation of stop-and-go traffic, accelerations, decelerations, and idling periods, allowing for an accurate assessment of a vehicle's emissions and fuel consumption in urban areas. The Braunschweig driving cycle includes frequent stops and starts to simulate the stop-and-go traffic commonly experienced in urban areas. This phase involves a series of accelerations, decelerations, and brief idling periods, reflecting the traffic congestion and traffic light patterns found in city driving. The driving cycle also includes an urban cruising phase, which represents steady-state driving at lower speeds on urban roads. This phase accounts for situations where vehicles maintain a consistent speed in areas with less traffic congestion, such as residential streets or lower speed limit zones.

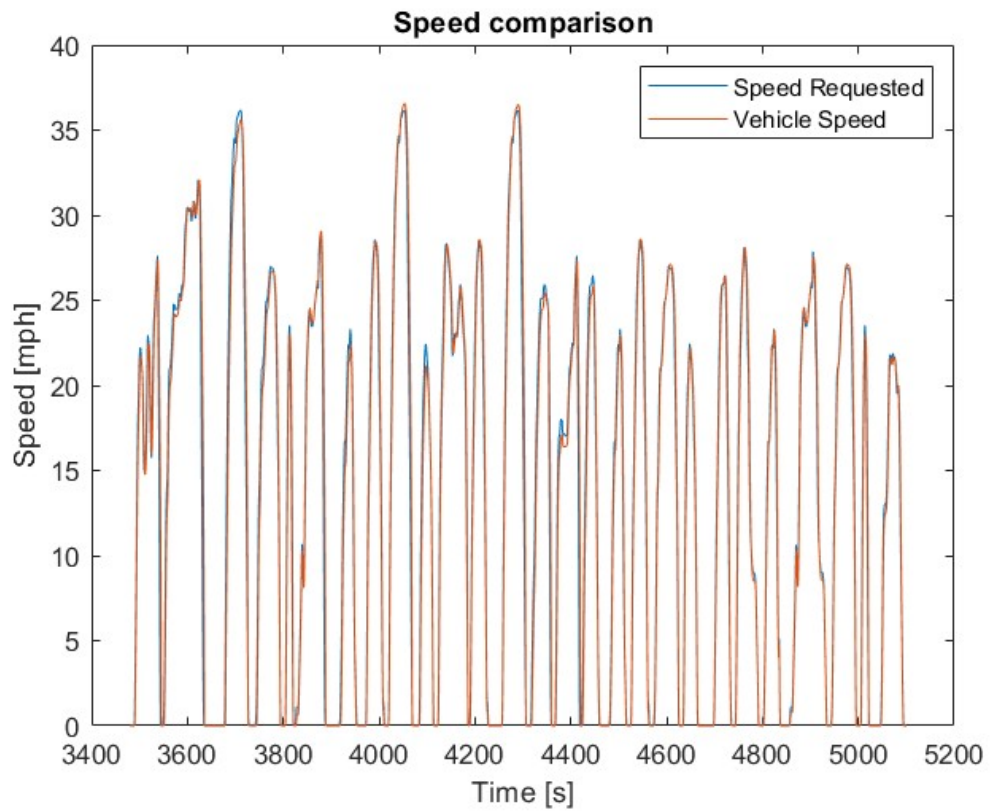


Figure 6.7: Speed requested vs Vehicle speed - BRAUNSCHWEIG

Being a much more aggressive driving cycle than the previous two, it can be seen much more zigzagging trends in the next graphs 6.7. This is due to the greater amount of braking, acceleration and higher average speeds.

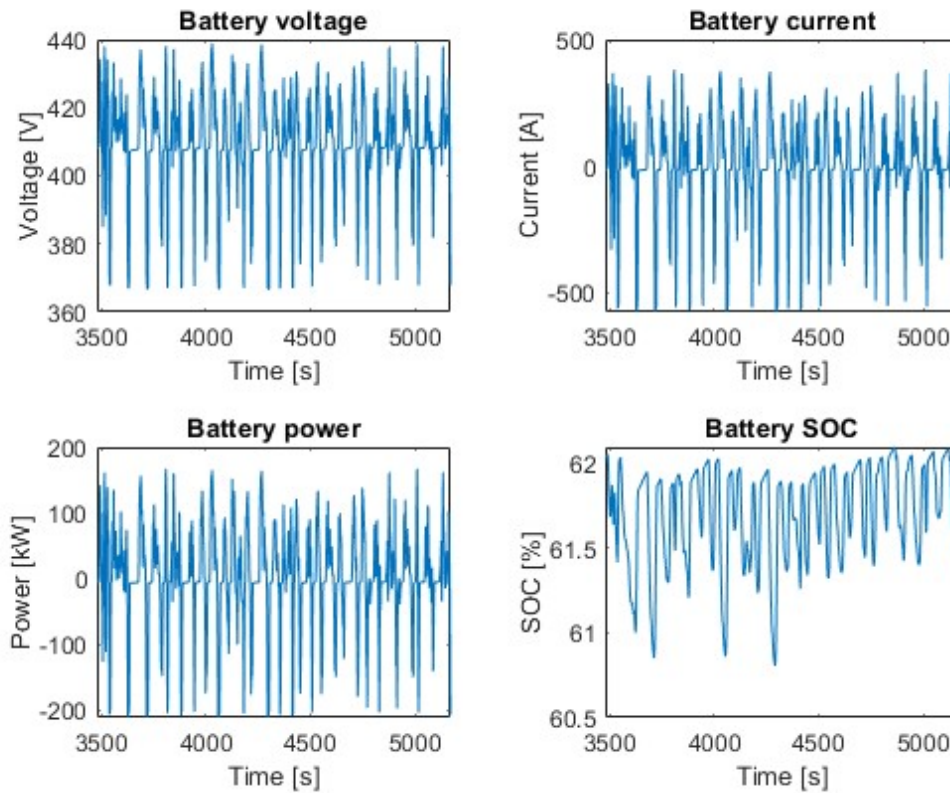


Figure 6.8: Battery parameters - BRAUNSCHWEIG (sign convention: +discharge -charge)

This feature can also be observed in the power balance in fig. 6.9, where it is possible to notice how the fuel cell reacts to a more dynamic driving cycle and with a higher average speed. There is a greater discharge of the battery and a greater use of the fuel cell as a battery charger, this is demonstrated by the higher output power from the fuel cell compared to the previous cases.

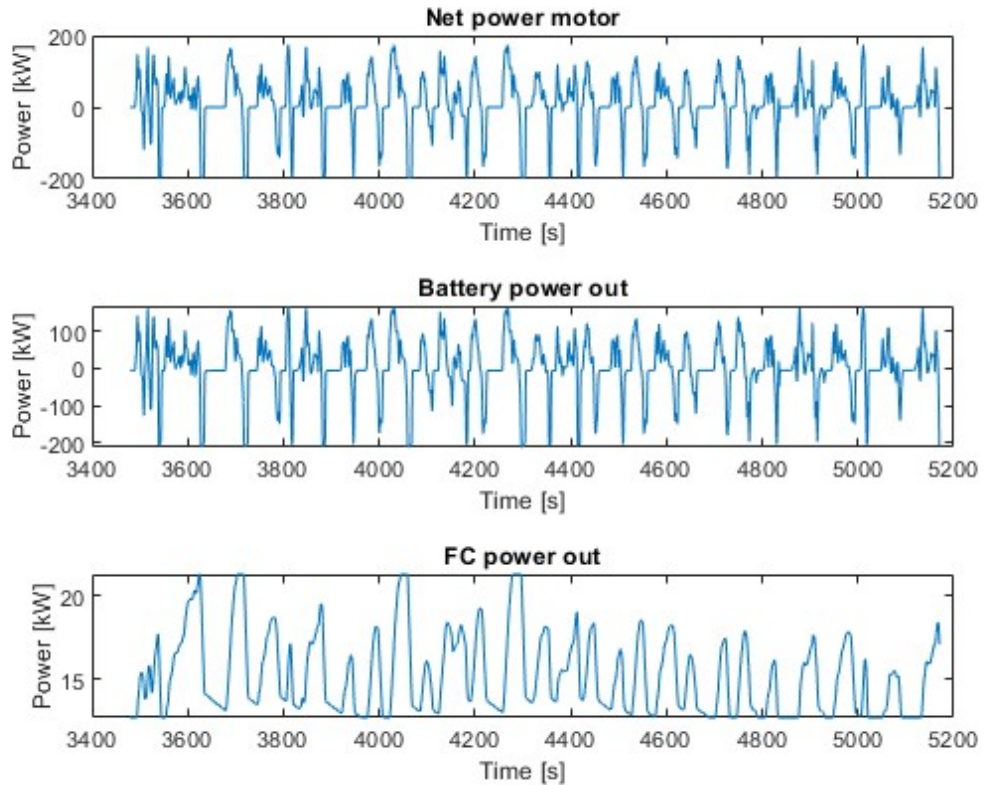


Figure 6.9: Power balance - BRAUNSCHWEIG (sign convention: +discharge -charge)

6.4 Aging results

Using the formula 3.9, the 3 curves present in 6.10 were obtained, which represent the aging of the battery following one of the 3 different driving cycles: Sort 1, Sort 2 and Braunschweig. Through the Braunschweig the battery life is longer than the SORT 1 and 2. This is explained by a lower use of the battery during this type of cycle, since, although more aggressive, the fuel cell is used more to compensate for the power peaks required. Instead, for the fuel cells the statements made at the end of chapter 4 are taken up again. Through the aging equation 4.3 for the fuel cell, used in this thesis, it was possible to obtain the necessary k ($k=0.43190$) backwards. In particular, it has been assumed that for SORT 1 the residual life of the fuel cell is 10,000 hours, similar to that of a hypothetical fuel cell vehicle today. After having obtained this k , it was then used on SORT 2 and Braunschweig obtaining the values shown in the table 6.1. These values, then multiplied by the average speed of the driving cycle, are able to give an idea of the hypothetical

residual life that the fuel cell could face.

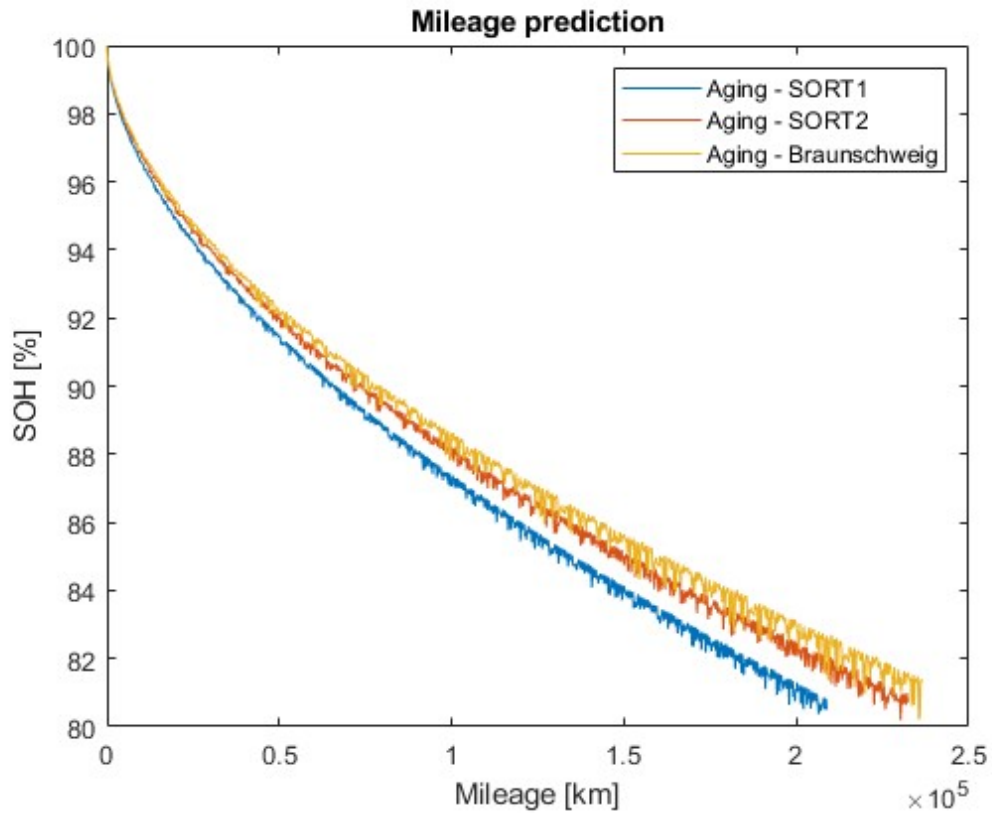


Figure 6.10: Aging for three different driving cycles Sort 1, Sort 2 ,Braunschweig

Table 6.1: FC residual lifetime and average speed

	Residual lifetime[h]	Average speed[km/h]	FC Mileage[km]
SORT 1	10000	12.0355	120355
SORT 2	9893.29	17.9537	177621
Braunschweig	7267.02	22.6729	164764

From table 6.1, it is therefore possible to obtain an overview of the aging of the fuel cell electric vehicle, comparing the aging of the battery and that of the fuel cell.

The result in 6.2 shows a large difference between fuel cell aging between SORT1 and SORT 2 . The reason lies in the empirical formula used, in which, with the assumptions made, the only variable terms between one case and another are the values of the working conditions and the power supplied by the fuel cell is not

Table 6.2: Aging mileage for battery and FC

	Battery Mileage [<i>km</i>]	FC Mileage [<i>km</i>]
SORT 1	208788	120355
SORT 2	232328	177621
Braunschweig	236036	164764

taken into consideration. This therefore implies that the residual life in the two cycles is quite similar, due to the values of the very similar working conditions, and this makes the product with the average speed even more influential. In the case of SORT 2, in fact, the average speed is quite higher than that of SORT 1, and this leads to a longer residual life.

Therefore, rather than giving an overview of the fuel cell's mileage, an estimate of its operational life in years of service would make more sense. Assuming an average use of the bus of 8 hours a day for about 340 days a year, an operating life in years like the one shown in table 6.3 is obtained.

Table 6.3: FC residual lifetime in years

	FC residual lifetimee [<i>hours</i>]	FC residual lifetime [<i>years</i>]
SORT 1	10000	3.67647
SORT 2	9893.29	3.63723
Braunschweig	7267.02	2.67169

Chapter 7

Conclusions

This work focused on the development of an FC electric vehicle model, with the electrical characterization of the battery and a study of the aging of both the battery and the fuel cell. The following conclusions can be drawn:

- The results obtained generally reflect what aging could be in a bus of this type. Nevertheless this work can be replicated for an aircraft or any other vehicle that wants to implement this technology (FC+battery). In particular, today there is the problem of high c-rates which shorten the operating life of components such as the battery and fuel cell.
- The proposed model is quite useful for the characterization of different driving cycles. It allows the analysis of the electrical behavior through the visualization of the electrical parameters, trend of the soc and moreover it supplies information on the power balances.
- The present work tries to analyze the aging mechanisms both in batteries and in fuel cells, and with fairly simple models it also tries to give a hypothetical reference value on the life of the just mentioned power sources.
- The proposed model does not use the influence of temperature in the fuel cell as it does not affect its performance much. Potentially, temperature dependence could be implemented in the battery but in the case of this thesis it was assumed constant as no data in relation to temperature were available. This factor could be decisive, as we have seen, in the mechanisms of degradation of the components, shortening their residual life.

The final goal of this thesis was to give an overview of how to develop a complete FC electric vehicle model and what are the aspects to take into consideration when doing a study of this type. Surely this study could be more in-depth, making the model capable of arriving at more accurate results, for example by taking into

consideration the influence of temperature or the variation of the RC parameters as a function of the state of charge (SOC) and the temperature, or else find different models from those used in this thesis. Finally, progress still needs to be made as regards the life of fuel cells and their technology in general, because in the panorama of propulsion, both in the automotive field and in others, a technology of this kind, to date, represents the future of transport.

Appendix A

Matab Script

```
1 % Run this file to see the results
2
3 clear all;           % Initialize workspace
4 close all;          % Close graphic windows
5
6 %%%%%%%%%%%%%%%%%%%%%%%%%%%%%%%%%%%%%%%%%%%%%%%%%%%%%%%%%%%%%%%%%%%%%%%%%
7 %load initialization data file
8 %%%%%%%%%%%%%%%%%%%%%%%%%%%%%%%%%%%%%%%%%%%%%%%%%%%%%%%%%%%%%%%%%%%%%%%%%
9 bus12m_sim_data ;
10 energy_manager_sim_data ;
11 FC_sim_data ;
12 Thermal_sim_data ;
13 battery_parameters ;
14
15 disp('Data loaded sucessfully!') ;
16
17 %%%%%%%%%%%%%%%%%%%%%%%%%%%%%%%%%%%%%%%%%%%%%%%%%%%%%%%%%%%%%%%%%%%%%%%%%
18 %Simulation initial conditions
19 %%%%%%%%%%%%%%%%%%%%%%%%%%%%%%%%%%%%%%%%%%%%%%%%%%%%%%%%%%%%%%%%%%%%%%%%%
20     ess_init_soc = 0.6;
21
22 %%%%%%%%%%%%%%%%%%%%%%%%%%%%%%%%%%%%%%%%%%%%%%%%%%%%%%%%%%%%%%%%%%%%%%%%%
23 %%%%%%%%%% load driving cycle %%%%%%%%%%
24 %%%%%%%%%%%%%%%%%%%%%%%%%%%%%%%%%%%%%%%%%%%%%%%%%%%%%%%%%%%%%%%%%%%%%%%%%
25 drivingcycle = 1; %1: Sort 1 %2: Sort 2 %3: Braunschweig
26 from_kmh_to_mph=1.609;
27 switch (drivingcycle)
28     case 1
29         %load SORT1
30         load CYC_SORT1.mat; % Load SORT 1 driving cycle
31         Speed_Req = [cyc_mph(:,1) ,cyc_mph(:,2)]/from_kmh_to_mph];
```

```

32     time_final = (cyc_mph(2,1)-cyc_mph(1,1))*length(cyc_mph(:,2))
    -(cyc_mph(2,1)-cyc_mph(1,1));
33
34     case 2
35         %load SORT2
36         load CYC_SORT2.mat; % Load SORT 2 driving cycle
37         Speed_Req = [cyc_mph(:,1),cyc_mph(:,2)/from_kmh_to_mph];
38         time_final = (cyc_mph(2,1)-cyc_mph(1,1))*length(cyc_mph(:,2))
    -(cyc_mph(2,1)-cyc_mph(1,1));
39
40     case 3
41         %load Braunschweig
42         load CYC_Braunschweig.mat % Load Braunschweig driving cycle
43         Speed_Req = [cyc_mph(:,1),cyc_mph(:,2)/from_kmh_to_mph];
44         time_final = (cyc_mph(2,1)-cyc_mph(1,1))*length(cyc_mph(:,2))
    -(cyc_mph(2,1)-cyc_mph(1,1));
45
46     end
47
48     %%%%%%%%%%%%%%%%%%%%%%%%%%%%%%%%%%%%%%%%%%%%%%%%%%%%%%%%%%%%%%%%%%%%%%%%%
49     % driver controller parameters
50     %%%%%%%%%%%%%%%%%%%%%%%%%%%%%%%%%%%%%%%%%%%%%%%%%%%%%%%%%%%%%%%%%%%%%%%%%
51     Kf_c = 1/10;
52     Kp_c = 30;
53     Ki_c = 1;
54     Ti_c = 60;
55     Tt_c = 65;
56     v_max_c = 100;
57
58
59     %%%%%%%%%%%%%%%%%%%%%%%%%%%%%%%%%%%%%%%%%%%%%%%%%%%%%%%%%%%%%%%%%%%%%%%%%
60     % BATTERY CONTROL
61     %%%%%%%%%%%%%%%%%%%%%%%%%%%%%%%%%%%%%%%%%%%%%%%%%%%%%%%%%%%%%%%%%%%%%%%%%
62     %%% SOC boundaries
63     high_soc=0.95; % highest desired battery state of charge
64     low_soc=0.10; % below this value, the engine must be on and charge
65     stop_soc=0.10; % lowest desired battery state of charge, avoid
    reaching this point
66     regstop_soc=0.9; % reach this point, regenerative brake will stop
67     P_aux=7500; % Auxiliary power
68
69     %%%%%%%%%%%%%%%%%%%%%%%%%%%%%%%%%%%%%%%%%%%%%%%%%%%%%%%%%%%%%%%%%%%%%%%%%
70     % Simulation and Results
71     %%%%%%%%%%%%%%%%%%%%%%%%%%%%%%%%%%%%%%%%%%%%%%%%%%%%%%%%%%%%%%%%%%%%%%%%%
72     time_step = 0.01;
73     sim('FCEV_v2.mdl');
74     disp('Simulation completed!');
75     bus12m_plot;
76     weight_factors;

```

Appendix B

Simulink design optimization toolbox

The Simulink Design Optimization Toolbox provides several optimization algorithms for estimating the parameters of a Simulink model. One of the most commonly used algorithms is the gradient-based optimization algorithm.

The gradient-based optimization algorithm uses the gradient of the objective function with respect to the design parameters to iteratively update the values of the parameters. The objective function is typically a measure of how well the model fits the data or meets certain performance criteria.

During each iteration of the algorithm, the gradient of the objective function is computed using numerical differentiation or automatic differentiation. The step size is then determined using a line search algorithm or a trust region method. The updated parameter values are then computed using the current parameter values, the gradient, and the step size.

The optimization algorithm continues to iterate until a stopping criterion is met, such as a maximum number of iterations or a convergence tolerance. Once the algorithm converges, the optimal parameter values are obtained.

Overall, the gradient-based optimization algorithm is a powerful tool for estimating the parameters of Simulink models. It can efficiently optimize a wide range of objective functions and is widely used in engineering and scientific applications.

Appendix C

Driving cycles

C.1 Constant driving - 160kph

This is a driving cycle, present among volkswagen data, which simulates driving with an approximately constant speed

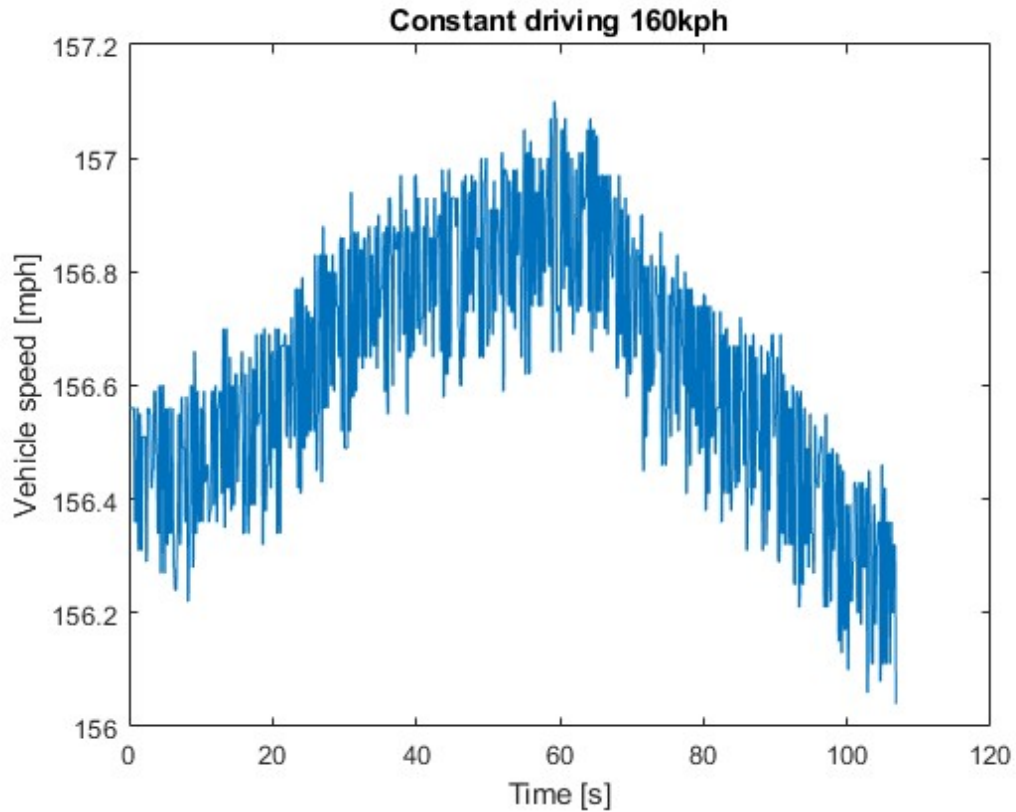


Figure C.1: Speed profile - Constant driving 160 kph

C.2 WLTP

The WLTP driving cycle is a comprehensive and standardized procedure used to evaluate the performance and emissions of light vehicles, including passenger cars and light commercial vehicles. It aims to reflect real-world driving conditions more accurately and considers a wide range of driving scenarios to provide a comprehensive assessment of vehicle efficiency and emissions.

The WLTP driving cycle consists of four different driving phases, each representing specific driving conditions commonly encountered on the road:

- **Low-Speed Driving Phase:** The driving cycle starts with a low-speed phase, which simulates urban driving conditions. It includes frequent stops, accelerations, and decelerations to mimic city traffic patterns. This phase assesses the vehicle's performance in stop-and-go situations and measures the associated fuel consumption and emissions.

- **Medium-Speed Driving Phase:** Following the low-speed phase, the medium-speed driving phase represents driving conditions encountered in suburban areas or on rural roads. It includes a combination of steady-speed driving, moderate accelerations, and decelerations. This phase evaluates the vehicle's efficiency under steady-state driving conditions and measures the corresponding fuel consumption and emissions.

- **High-Speed Driving Phase:** The high-speed driving phase simulates driving conditions on highways and motorways. It involves sustained high-speed driving, with occasional accelerations and decelerations. This phase assesses the vehicle's performance at higher speeds and measures fuel consumption and emissions accordingly.

- **Extra-High-Speed Driving Phase:** The extra-high-speed driving phase represents situations where vehicles operate at very high speeds, such as during overtaking maneuvers. It involves brief periods of intense acceleration and deceleration. This phase evaluates the vehicle's performance under extreme driving conditions and measures the associated fuel consumption and emissions.

The total duration of the WLTP driving cycle is approximately 30 minutes, which is divided among the different driving phases according to their respective durations in real-world driving conditions.

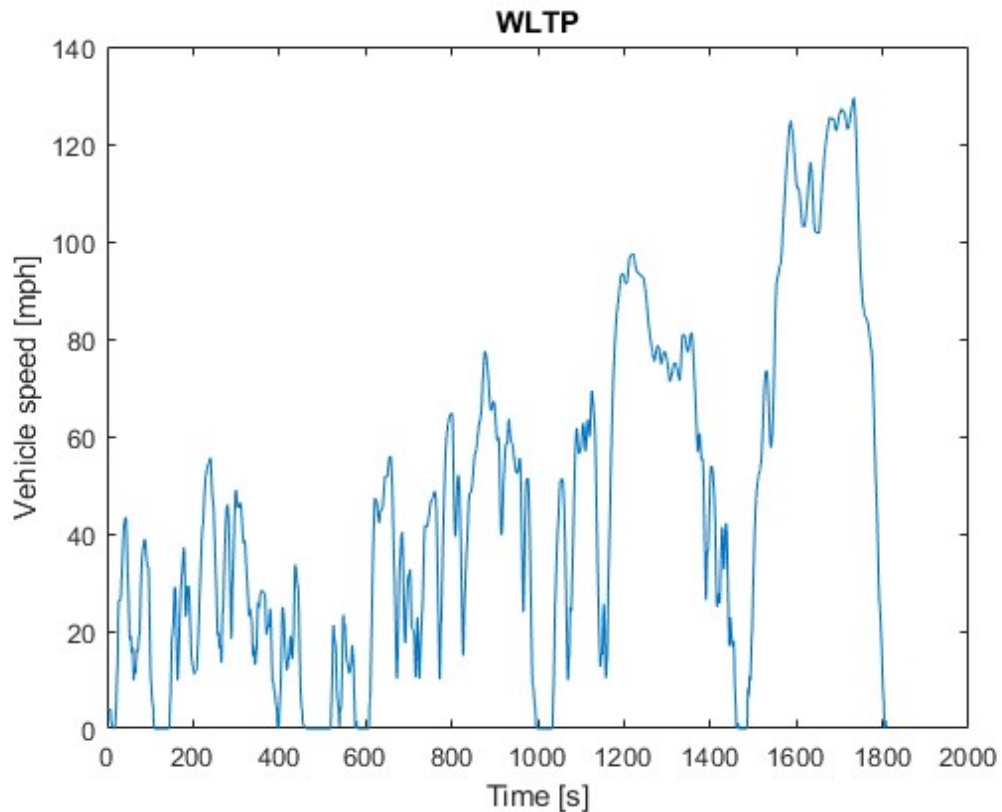


Figure C.2: Speed profile - WLTP

C.3 FTP

The FTP driving cycle is designed to represent urban driving conditions commonly encountered in the United States. It consists of two main driving phases: the Urban Driving Schedule (UDS) and the Highway Fuel Economy Driving Schedule (HFEDS). These phases simulate different driving scenarios and aim to provide a comprehensive evaluation of a vehicle's emissions and fuel consumption.

- **Urban Driving Schedule (UDS):** The UDS phase of the FTP driving cycle represents typical stop-and-go city driving conditions. It includes various driving maneuvers, such as accelerations, decelerations, idling, and steady-state driving. The UDS phase evaluates a vehicle's performance in urban traffic and measures the associated emissions and fuel consumption.
- **Highway Fuel Economy Driving Schedule (HFEDS):** The HFEDS phase of the FTP driving cycle simulates driving conditions on highways and represents steady-state cruising at higher speeds. It involves maintaining a constant

speed for an extended period, without frequent accelerations or decelerations. The HFEDS phase assesses a vehicle's fuel efficiency during highway driving and measures the corresponding emissions.

The total duration of the FTP driving cycle is approximately 1,187 seconds, with the UDS phase lasting 900 seconds and the HFEDS phase lasting 287 seconds. The duration is selected to represent typical driving patterns and provide a reliable assessment of vehicle performance.

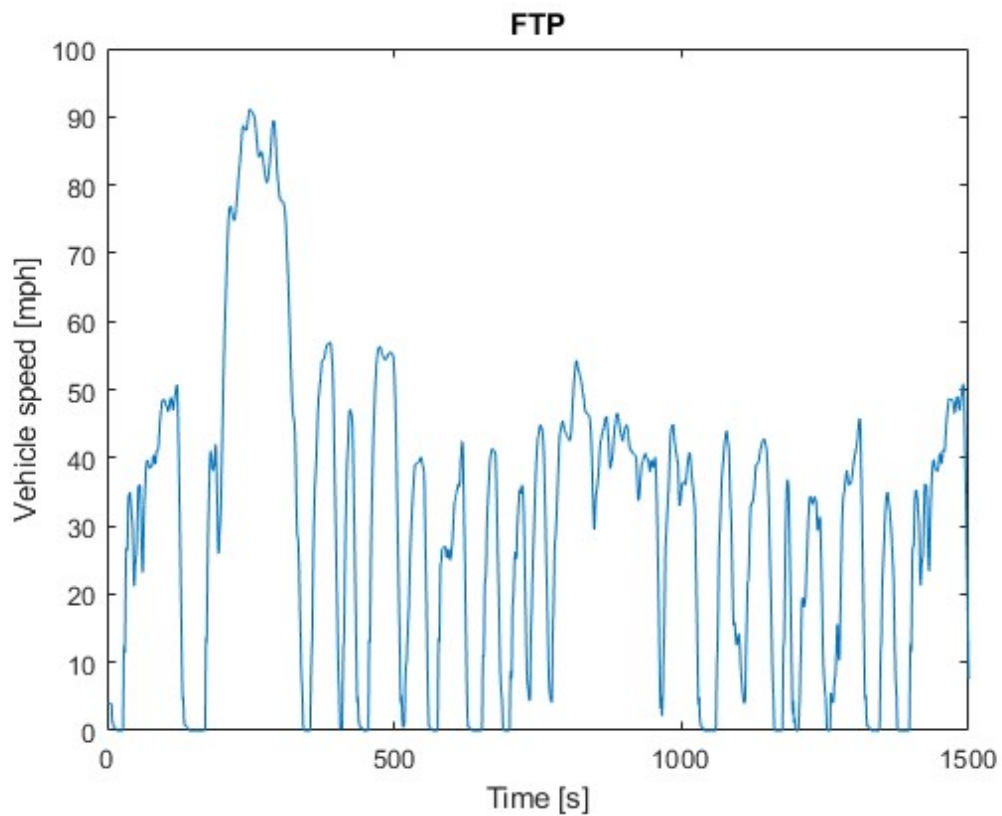


Figure C.3: Speed profile - FTP

C.4 Urban

This is a driving cycle, present among volkswagen data, which simulates driving in an urban environment with low average speeds

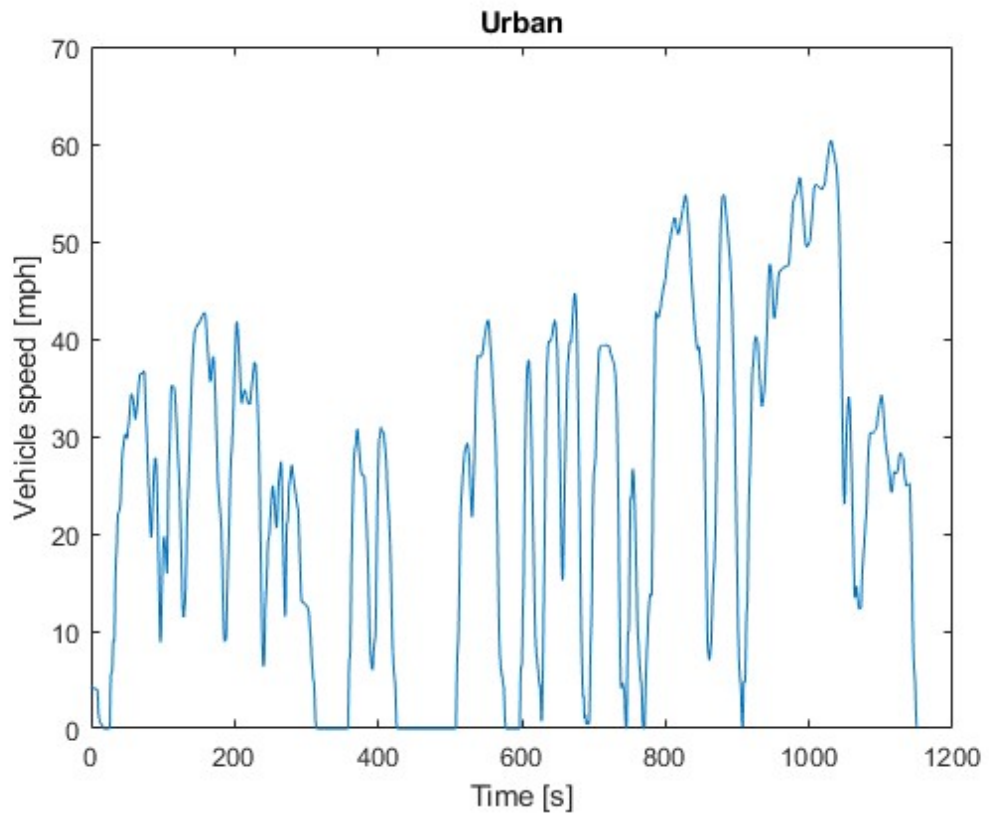


Figure C.4: Speed profile - Urban

C.4.1 Interurban

This is a driving cycle, present in volkswagen data, which simulates driving in an intercity environment with average speeds

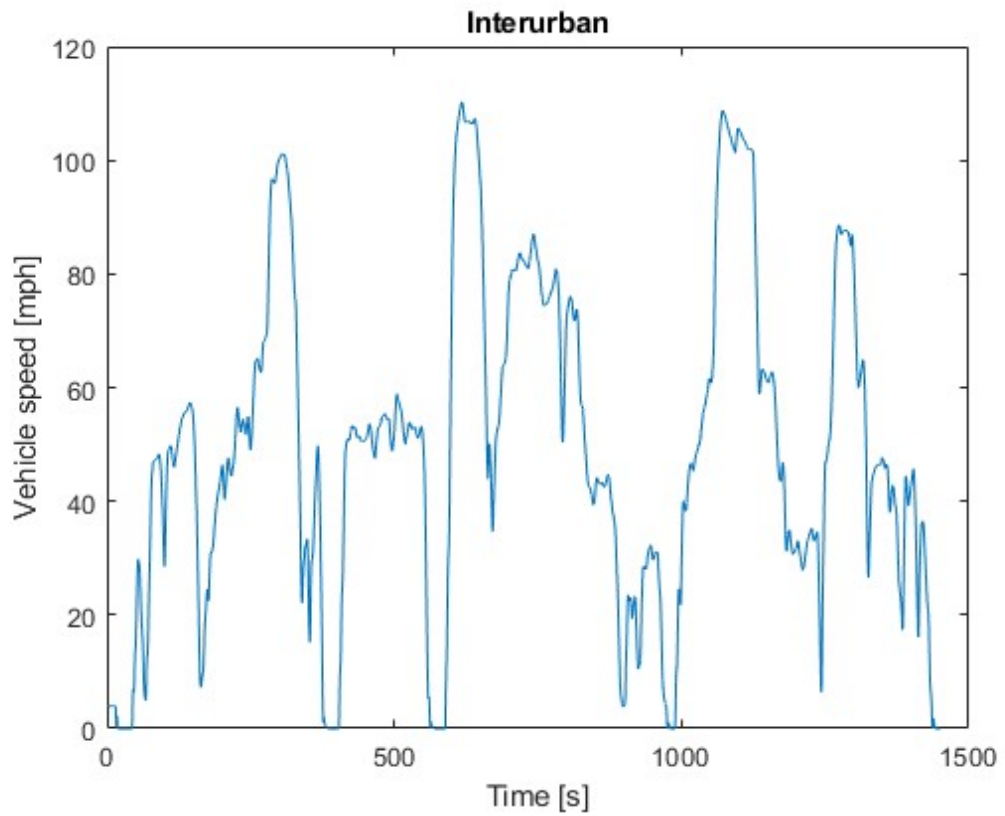


Figure C.5: Speed profile - Interurban

C.4.2 Highway

This is a driving cycle, present in volkswagen data, which simulates driving in a highway environment with high speeds

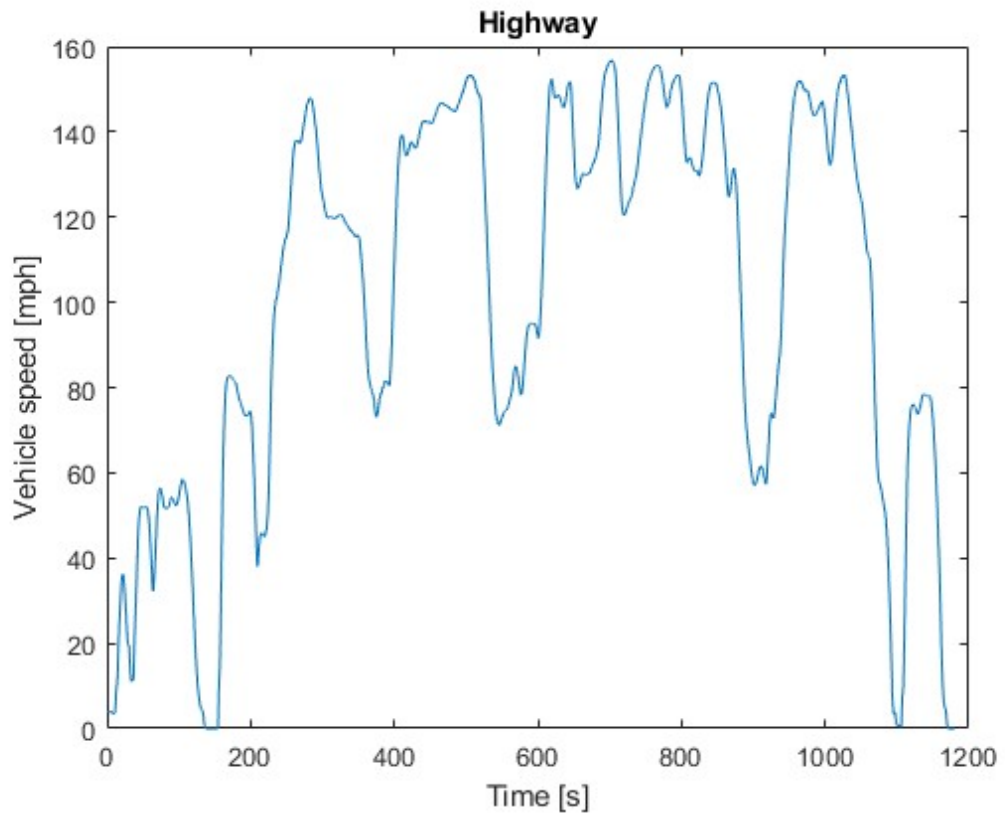


Figure C.6: Speed profile - Highway

Bibliography

- [1] Frederik Vorholt Vera Beermann. European battery cell production expands. https://www.ipcei-batteries.eu/fileadmin/Images/accompanying-research/market-updates/2022-01-BZF_Kurzinfo_Marktanalyse_Q4_ENG.pdf, 2021.
- [2] Matthew Roberts Euan McTurk Peter G. Bruce Christoph Birkl, Brill Power. Degradation diagnostics for lithium ion cells. *Journal of Power Sources*, pages 373–386, 2017.
- [3] Global Footprint Network. Population growth. <https://www.footprintnetwork.org/>, 2022.
- [4] Stijn Pauwelsd Marcel Meeuse Filip Leemansa Bavo Verbruggeb Wouter De Nijs d Peter Van den Bosschec Daan Sixa Joeri Van Mierlob Grietus Muldera, Noshin Omarb. Comparison of commercial battery cells in relation to material properties. *Elsevier, Oxford*, pages 473–488, 2012.
- [5] SP Global. The future of battery technology. <https://www.spglobal.com/esg/s1/topic/the-future-of-battery-technology.html>, 2021.
- [6] M.Nikdel S.M. MousaviG. n. Various batterymodelsforvariousimulationstudiesandapplications. *Renewable and Sustainable Energy Reviews*, pages 477–485, 2014.
- [7] Steinsträter M. Schreiber M. Rosner P. Nicoletti L. Schmid F. Ank M. Teichert O. Wildfeuer L. Schneider J. Koch A. König A. Glatz A. Gandlgruber J. Kröger T. Lin X. Lienkamp M. Wassiliadis, N. Quantifying the state of the art of electric powertrains in battery electric vehicles: Range, efficiency, and lifetime from component to system level of the volkswagen id.3. *eTransportation*, 2022.
- [8] Kun Li Zhen Zhao Huixin Tian, Pengliang Qin. A review of the state of health for lithium-ion batteries: Research status and suggestions. *Journal of Cleaner Production*, 2020.
- [9] Gilbert Laporte Marco Veneroni Samuel Pelletier, Ola Jabali. Battery degradation and behaviour for electric vehicles: Review and numerical analyses of several models. *Transportation Research Part B*, pages 158–187, 2017.
- [10] Simona Onori Girish Suri. A control-oriented cycle-life model for hybrid electric vehicle lithium-ion batteries. *Energy*, pages 644–659, 2016.

- [11] Stefano Marelli and Simona Onori. Multi-objective supervisory controller for hybrid electric vehicles. *Automotive Research*, page Chapter 9, 2016.
- [12] Jonathan J. Martin Haijiang Wang Jiujun Zhang Jun Shen Shaohong Wu Walter Merida Jinfeng Wu, Xiao Zi Yuan. A review of pem fuel cell durability: Degradation mechanisms and mitigation strategies. *Journal of Power Sources*, pages 104–119, 2008.
- [13] Xiao Hu Ke Song, Yimin Wang and Jing Ca. Online prediction of vehicular fuel cell residual lifetime based on adaptive extended kalman filter. *energies*, 2020.